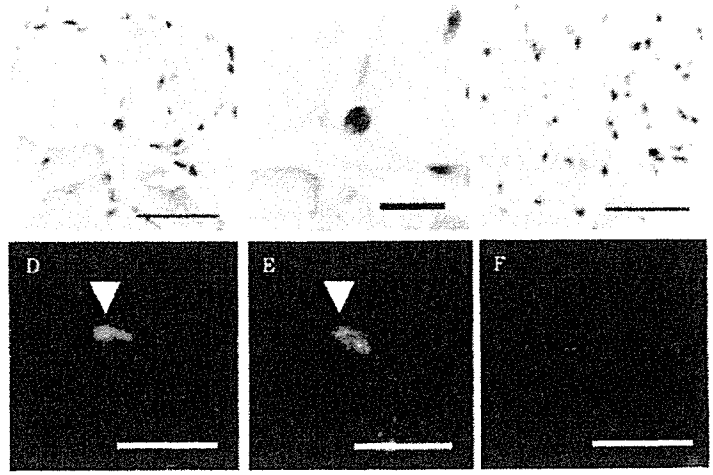

Fig. 3. HGF immunolocalization in reloaded soleus muscle. The upper row (A–C) shows immunoperoxidase. Arrows indicate HGF in the cytoplasm of small cells contiguous to muscle fibers (A, B). The lower row (D–F) shows immunofluorescence. E and F: nuclei (blue) are observed surrounding muscle fibers. D and E: HGF (green) is localized in satellite cells surrounding adjacent muscle fibers (arrows). Negative controls stained using normal rabbit serum did not display positive results for HGF (C, F). Scale bar, 30 μm in A and C, 10 μm in B and 20 μm in D–F.

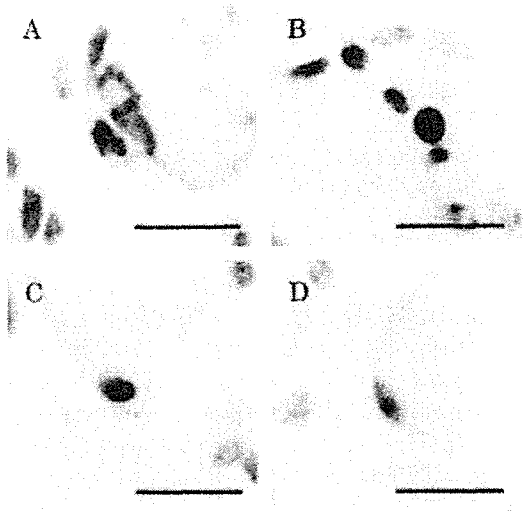

Fig. 4. Immunohistochemical localization for c-Met and PCNA in reloaded soleus muscle. Positive results for c-Met are apparent in small cells contiguous with muscle fibers (arrow). Myogenic nuclei (A) in a similar position display positive reactivity to PCNA, suggesting that these cells represent activated satellite cells (arrow). PCNA-positive cells (C) are present along with mononuclear cells. Negative controls stained using normal rabbit serum or normal mouse serum did not display positive results for c-Met or PCNA (B, D). Scale bar, 10 μm.

found that the mass of both soleus and plantaris muscles in rats decreased following hindlimb suspension for 2 weeks. Atrophy might be caused by myonuclear cell apoptosis[9, 35, 36], reduced protein synthesis[41] or activation of proteolytic systems such as the ubiquitin-proteasome system[37, 38], calpain system[39] and cathepsin D system[5]. The masses of both muscles normalized after 3 days of reloading following the 2 weeks of unloading. Thus, both soleus and plantaris muscles are able to recover following atrophy. However, the process leading to recovery seems to differ, with degeneration and regeneration occurring in the recovery process in the soleus muscle, but not in the plantaris muscle. Previous studies have reported that numbers of myonuclear cells per unit area increase following reloading of atrophied soleus muscle[8, 9, 40, 41] and this was also observed in the present study. The soleus muscle is known as an antigravity muscle containing slow-twitch fibers. ATPase staining shows that proportions of muscle fiber types differ between the soleus and plantaris muscles. Analysis of myosin heavy chain (MHC) isoforms has likewise indicated a difference, showing 40–70% MHC type I in mouse soleus muscle corresponding to type I fibers[42, 43], while mouse plantaris muscle contains predominantly type IIa and IIB MHCs

corresponding to type II fibers[44]. Electromyography shows that muscle activity in the rat soleus muscle increases during treadmill locomotion after hindlimb unloading[45]. Although the precise mechanisms are unknown, differing processes may be related to these differences in muscle fiber types. In addition, satellite cells are central to regeneration and could explain how these differences contribute to the process of degeneration and regeneration. Previous studies have reported that satellite cells comprise approximately 2% of the myonuclear population in the tibialis anterior muscle of 4-month-old mice and 9.6% in the soleus muscle of 1-month-old rats[11, 46]. Furthermore, mitotic activity of satellite cells in the soleus muscle is 0.052% in 24-month-old rats[47]. These findings show that slow muscles display a higher number of satellite cells than other muscles.

Reloading increased the level of HGF in the soleus muscle by approximately 3-fold compared to controls. This agrees with a previous report that HGF levels in rat quadriceps muscles increase in response to muscle injury[32]. Patterns of local injury, such as infiltration of macrophages and degeneration of muscle fibers and central nuclear cells, were observed following reloading of the soleus muscle. We also found that the HGF appears to be present in satellite cells surrounding uninjured small muscle fibers. Previous studies have reported that HGF is present in the extracellular matrix surrounding muscle fibers[16, 48], or immunolocalized at regenerating skeletal muscle[49]. In situ hybridization has also revealed HGF mRNA in regenerating muscle fibers[15, 31]. In the present study, HGF was clearly immunolocalized in the cytoplasm of satellite cells early in the recovery process, strongly suggesting that HGF is produced by local satellite cells in response to reloading stimulation. Muscle fiber injury induces macrophage infiltration, but HGF mRNA is not present in macrophages, as demonstrated by Jennische et al.[15] and the present study. Furthermore, c-Met was expressed in the cell membranes of satellite cells. Satellite cells display c-Met in all states of activation, proliferation and differentiation[27] and c-Met can be used as a molecular marker for these cells. The satellite cell is known as a quiescent muscle progenitor cell, and injury leads to cell activation[50]. After reloading, the majority of satellite cells were PCNA-positive, indicating that cells had entered the cell cycle. HGF- and HGF-receptor-positive cells are thus activated satellite cells. Taken together, recovery appears to be partially accomplished by proliferation and maturation of satellite cells, and proliferation of satellite cells seems likely to occur in an autocrine or paracrine manner with satellite cells producing HGF, followed by HGF activating the HGF-receptor-positive cells, satellite cells.

In conclusion, these results suggest that HGF production, stimulated in satellite cells, is the cause of recovery following mechanical stimulation in disuse-atrophied muscle.

ACKNOWLEDGEMENTS

We would like to thank Prof. Toshio Nakatani from the Division of Health Sciences, Graduate School of Medical Science, Kanazawa University for supporting the present study.

REFERENCES

1) Widrick JJ, Romatowski JG, Norenberg KM, et al.: Functional properties of slow and fast gastrocnemius muscle fibers after a 17-day spaceflight. J Appl Physiol, 2001, 90: 2203–2211.
2) Booth FW, Gollnick PD: Effects of disuse on the structure and function of skeletal muscle. Med Sci Sports Exerc, 1983, 15: 415–420.
3) Eichelberger L, Roma M, Moulder PV: Effects of immobilization atrophy on the histochemical characterization of skeletal muscle. J Appl Physiol, 1958, 12: 42–50.
4) Howard G, Steffen JM, Geoghegan TE: Transcriptional regulation of decreased protein synthesis during skeletal muscle unloading. J Appl Physiol, 1989, 66: 1093–1098.
5) Taillandier D, Aurousseau E, Combaret L, et al.: Regulation of proteolysis during reloading of the unweighted soleus muscle. Int J Biochem Cell Biol, 2003, 35: 665–675.
6) Mozdziak PE, Pulvermacher PM, Schultz E: Muscle regeneration during hindlimb unloading results in a reduction in muscle size after reloading. J Appl Physiol, 2001, 91: 183–190.
7) Rosenblatt JD, Yong D, Parry D: Satellite cell activity is required for hypertrophy of overloaded adult rat muscle. Muscle Nerve, 1994, 17: 608–613.
8) Smith HK, Maxwell L, Rodfers CD, et al.: Exercise-enhanced satellite cell proliferation and new myonuclear accretion in rat skeletal muscle. J Appl Physiol, 2001, 90: 1407–1414.
9) Allen DL, Roy RR, Edgerton VR: Myonuclear domains in muscle adaptation and disease. Muscle Nerve, 1999, 22: 1350–1360.

10) Mauro A: Satellite cells of skeletal muscle fibers. J Cell Biol, 1961, 9: 493–495.
11) Schultz E, Gibson MC, Champion T: Satellite cells are mitotically quiescent in mature mouse muscle: an EM and radioautographic study (1). J Exp Zool, 1978, 206: 451–456.
12) Darr KC, Schultz E: Exercise-induced satellite cell activation in growing and mature skeletal muscle. J Appl Physiol, 1987, 63: 1816–1821.
13) Bischoff R: A satellite cell mitogen from crushed adult muscle. Dev Biol, 1986, 115: 140–147.
14) Snow MH: Myogenic cell formation in regenerating rat skeletal muscle injured by mincing, II. An autoradiographic study. Anat Rec, 1997, 188: 201–218.
15) Jennische E, Ekberg S, Matejka GJ: Expression of hepatocyte growth factor in growing and regenerating rat skeletal muscle. Am J Physiol Cell Physiol, 1993, 265: C122–C128.
16) Tatsumi R, Anderson JE, Nevoret CJ, et al.: HGF/SF is present in normal adult skeletal muscle and is capable of activating satellite cells. Dev Biol, 1998, 194: 114–128.
17) Cook DR, Doumit ME, Merkel RA: Transforming growth factor-beta, basic fibroblast growth factor, and platelet-derived growth factor-BB interact to affect proliferation of clonally derived porcine satellite cells. J Cell Physiol, 1993, 157: 307–312.
18) Doumit ME, Cook DR, Merkel RA: Fibroblast growth factor, epidermal growth factor, insulin-like growth factors, and platelet-derived growth factor-BB stimulate proliferation of clonally derived porcine myogenic satellite cells. J Cell Physiol, 1993, 157: 326–332.
19) Phelan JN, Gonyea WJ: Effect of radiation on satellite cell activity and protein expression in overloaded mammalian skeletal muscle. Anat Rec, 1997, 247: 179–188.
20) Kastner S, Elias MC, Rivera AJ, et al.: Gene expression patterns of the fibroblast growth factors and their receptors during myogenesis of rat satellite cells. J Histochem Cytochem, 2000, 48: 1079–1096.
21) Yablonka-Reuveni Z, Seger R, Rivera AJ: Fibroblast growth factor promotes recruitment of skeletal muscle satellite cells in young and old rats. J Histochem Cytochem, 1999, 47: 23–42.
22) Allen RE, Sheehan SM, Taylor RG, et al.: Hepatocyte growth factor activates quiescent skeletal muscle satellite cells in vitro. J Cell Physiol, 1995, 165: 307–312.
23) Wozniak AC, Kong J, Bock E, et al.: Signaling satellite-cell activation in skeletal muscle: markers, models, stretch, and potential alternate pathways. Muscle Nerve, 2005, 31: 283–300.
24) Nakamura T, Nawa K, Ichihara A: Partial purification and characterization of hepatocyte growth factor from serum of hepatectomized rats. Biochem Biophys Res Commun, 1984, 122: 1450–1459.
25) Tashiro K, Hagiya M, Nishizawa T, et al.: Deduced primary structure of rat hepatocyte growth factor and expression of the mRNA in rat tissues. Proc Natl Acad Sci U S A, 1990, 87: 3200–3204.
26) Nakamura T, Nishizawa T, Hagiya M, et al.: Molecular cloning and expression of human hepatocyte growth factor. Nature, 1989, 342: 440–443.
27) Cornelison DDW, Wold B: Single-cell analysis of regulatory gene expression in quiescent and activated mouse skeletal muscle satellite cells. Dev Biol, 1997, 191: 270–283.
28) Sheehan SM, Tatsumi R, Temm-Grove JJ: HGF is an autocrine growth factor for skeletal muscle satellite cells in vitro. Muscle Nerve, 2000, 23: 239–245.
29) Bottaro DP, Rubin JS, Faletto DL, et al.: Identification of the hepatocyte growth factor receptor as the c-met proto-oncogene product. Science, 1991, 251: 802–804.
30) Ferracini R, Longati P, Naldini L, et al.: Identification of the major autophosphorylation site of the Met/hepatocyte growth factor receptor tyrosine kinase. J Biol Chem, 1991, 266: 19558–19564.
31) Yamaguchi A, Ishii H, Morita I, et al.: mRNA expression of fibroblast growth factors and hepatocyte growth factor in rat plantaris muscle following denervation and compensatory overload. Pflugers Arch, 2004, 448: 539–546.
32) Suzuki S, Yamanouchi K, Soeta C, et al.: Skeletal muscle injury induces hepatocyte growth factor expression in spleen. Biochem Biophys Res Commun, 2002, 292: 709–714.
33) Morey-Holton ER, Globus RK: Hindlimb unloading rodent model: technical aspects. J Appl Physiol, 2002, 92: 1367–1377.
34) Diffee GM, Haddad F: Control of myosin heavy chain expression: interaction of hypothyroidism and hindlimb suspension. Am J Physiol Cell Physiol, 1991, 261: C1099–C1106.
35) Allen DL, Linderman JK, Roy RR, et al.: Apoptosis: a mechanism contributing to remodeling of skeletal muscle in response to hindlimb unweighting. Am J Physiol Cell Physiol, 1997, 273: C579–C587.
36) Siu PM, Pistilli EE, Butler DC, et al.: Aging influences cellular and molecular responses of apoptosis to skeletal muscle unloading. Am J Physiol Cell Physiol, 2005, 288: C338–C349.
37) Bodine SC, Latres E, Baumhueter S, et al.: Identification of ubiquitin ligases required for skeletal muscle atrophy. Science, 2001, 294: 1704–1708.
38) Price SR: Increased transcription of ubiquitin-proteasome system components: molecular responses associated with muscle atrophy. Int J Biochem Cell Biol, 2003, 35: 617–628.
39) Huang J, Forsberg NE: Role of calpain in skeletal-muscle protein degradation. Proc Natl Acad Sci U S A, 1998, 95: 12100–12105.
40) Nguyen HX, Tidball JG: Expression of a muscle-specific, nitric oxide synthase transgene prevents muscle membrane injury and reduces muscle

inflammation during modified muscle use in mice. J Physiol (Lond), 2003, 5502: 347–356.
41) Putman CT, Dusterhoft S, Pette D: Changes in satellite cell content and myosin isoforms in low-frequency-stimulated fast muscle of hypothyroid rat. J Appl Physiol, 1999, 86: 40–51.
42) Carlson CJ, Booth FW, Gordon SE: Skeletal muscle myostatin mRNA expression is fiber-type specific and increases during hindlimb unloading. Am J Physiol Regul Integr Comp Physiol, 1999, 277: R601–R606.
43) Jin T-E, Witzemann V, Brecht M: Fiber types of the intrinsic whisker muscle and whisking behavior. J Neurosci, 2004, 24: 3386–3393.
44) Miyazaki M, Hitomi Y, Kizaki T, et al.: Contribution of the calcineurin signaling pathway to overload-induced skeletal muscle fiber-type transition. J Physiol Pharmacol, 2004, 55: 751–764.
45) Canu MH, Falempin M: Effect of hindlimb unloading on two hindlimb muscles during treadmill locomotion in rats. Eur J Appl Physiol, 1997, 75: 283–288.
46) Gibson MC, Schultz E: Age-related differences in absolute numbers of skeletal muscle satellite cells. Muscle Nerve, 1983, 6: 574–580.
47) McCormick KM, Thomas DP: Exercise-induced satellite cell activation in senescent soleus muscle. J Appl Physiol, 1992, 72: 888–893.
48) Tatsumi R, Allen RE: Active hepatocyte growth factor is present in skeletal muscle extracellular matrix. Muscle Nerve, 2004, 30: 654–658.
49) Hayashi S, Aso H, Watanabe K, et al.: Sequence of IGF-I, IGF-II, and HGF expression in regenerating skeletal muscle. Histochem Cell Biol, 2004, 122: 427–434.
50) Grounds MD, White JD, Rosenthal N, et al.: The role of stem cells in skeletal and cardiac muscle repair. J Histochem Cytochem, 2002, 50: 589–610.

WILEY InterScience® DISCOVER SOMETHING GREAT

Journal of Neuroscience Research 84:874–890 (2006)

Possible Role of Scavenger Receptor SRCL in the Clearance of Amyloid-β in Alzheimer's Disease

Kenji Nakamura,[1] Wakana Ohya,[1] Hiroshi Funakoshi,[1] Gaku Sakaguchi,[3] Akira Kato,[3] Masatoshi Takeda,[2] Takashi Kudo,[2] and Toshikazu Nakamura[1]*

[1]Division of Molecular Regenerative Medicine, Department of Biochemistry and Molecular Biology, Osaka University Graduate School of Medicine, Osaka, Japan
[2]Psychiatry, Department of Integrated Medicine, Division of Internal Medicine, Osaka University Graduate School of Medicine, Osaka, Japan
[3]Pain and Neurology, Discovery Research Laboratories, Shionogi and Co., Ltd., Shiga, Japan

Accumulation of β-amyloid protein (Aβ) in the brain is a hallmark of Alzheimer's disease (AD), and Aβ-mediated pathogenesis could result from increased production of Aβ or insufficient Aβ clearance by microglia, astrocytes, or the vascular system. Cell-surface receptors, such as scavenger receptors, might play a critical role in the binding and clearing of Aβ; however, the responsible receptors have yet to be identified. We show that scavenger receptor with C-type lectin (SRCL), a member of the scavenger receptor family containing coiled-coil, collagen-like, and C-type lectin/carbohydrate recognition domains, is expressed in cultured astrocytes and microglia. In contrast to the low expression of SRCL in the wild-type mouse brain, in a double transgenic mouse model of AD (Tg-APP/PS1), immunohistochemistry showed that SRCL was markedly induced in Aβ-positive astrocytes and Aβ-positive vascular/perivascular cells, which are associated closely with cerebral amyloid angiopathy. In patients with AD, the distribution of SRCL was similar to that seen in the Tg-APP/PS1 temporal cortex. The presence of a large number of SRCL/Aβ double-positive particles in the intracellular compartments of reactive astrocytes and vascular/perivascular cells in Tg-APP/PS1 mice and AD patients suggests a role for SRCL in Aβ clearance. Moreover, CHO-K1 cells transfected with SRCL isoforms were found to bind fibrillar $A\beta_{1-42}$. These findings suggest that SRCL could be the receptor involved in the binding or clearing of Aβ by glial and vascular/perivascular cells in AD.

Key words: scavenger receptor; SRCL; amyloid-β; astrocytes; microglia

Alzheimer's disease (AD) is a progressive neurodegenerative disorder (Tanzi and Bertram, 2005) characterized by accumulation of β-amyloid protein (Aβ) in the brain, which accumulation is thought to play a key role in the pathogenesis of AD. Aβ-associated pathogenesis may arise from the increased production of Aβ, or insufficient Aβ clearance by microglia, astrocytes, or the vascular system (Nicoll and Weller, 2003; Tanzi et al., 2004; Zlokovic, 2004; Tanzi and Bertram, 2005). Microglia and astrocytes have the ability to clear Aβ (Paresce et al., 1996; Guenette, 2003a,b; Wyss-Coray et al., 2003). For example, cultured wild-type mouse astrocytes were shown to bind to and contribute to the clearance of Aβ in Aβ-laden fresh brain sections of a transgenic mouse model of AD (Wyss-Coray et al., 2003); and a variety of substances can modulate Aβ clearance by microglia, astrocytes, and the vasculature, including antibodies against Aβ-peptide, TGFβ1, heat-shock proteins, apolipoprotein E (apoE), a monoclonal antibody against Aβ, and GM1 (Bard et al., 2000; Wyss-Coray et al., 2001; DeMattos et al., 2002; Kakimura et al., 2002; Matsuoka et al., 2003; Koistinaho et al., 2004). Antibodies against Aβ-peptide triggered microglial cells to clear plaques through Fc receptor-mediated phagocytosis and subsequent peptide degradation (Bard et al., 2000). These data show that Aβ can be eliminated from the brain, directly by glial cells, directly into the blood by vascular cells, or indirectly along perivascular interstitial fluid drainage channels and that the efficiency of Aβ clearance can be regulated. It has been postulated that increasing Aβ clearance may be a promising thera-

Supplementary Material for this article is available online at http://www.mrw.interscience.wiley.com/suppmat/0360-4012/suppmat/(www.interscience.wiley.com).

Contract grant sponsor: COE; Contract grant sponsor: Ministry of Education, Science, Technology, Sports and Culture of Japan and Ministry of Health and Welfare of Japan.

*Correspondence to: Dr. Toshikazu Nakamura, Division of Molecular Regenerative Medicine, Department of Biochemistry and Molecular Biology, Osaka University Graduate School of Medicine, B-7, Osaka 565-0871, Japan. E-mail: nakamura@onbich.med.osaka-u.ac.jp

Received 22 November 2005; Revised 10 May 2006; Accepted 23 May 2006

Published online 25 July 2006 in Wiley InterScience (www.interscience.wiley.com). DOI: 10.1002/jnr.20992

peutic approach to reduce Aβ-mediated pathogenesis in AD. Cell-surface receptors, such as scavenger receptors and related molecules, may play a critical role in the binding and clearance of Aβ; however, the putative receptors responsible for Aβ clearance have not yet been clearly identified (Paresce et al., 1996; Shibata et al., 2000; El Khoury et al., 2003; Alarcon et al., 2005).

Scavenger receptor with C-type lectin (SRCL) (Nakamura et al., 2001a, 2001b) is a member of the scavenger receptor (SR) family (Murphy et al., 2005), which members contain coiled-coil, collagen-like, and C-type lectin/carbohydrate recognition (CRD) domains. The predominant form of SRCL in humans was named human SRCL Type I (hSRCL-I). In contrast, the SRCL containing coiled-coil and collagen-like domains but lacking the CRD domain was termed human SRCL Type II (hSRCL-II) (Nakamura et al., 2001a). Because of structural similarities, SRCL is considered to be closely related to the Class A scavenger receptor (SR-A), which contains coiled-coil, collagen-like, and cysteine-rich domains (Kodama et al., 1990). The ability of SRCLs to bind Gram-negative and Gram-positive bacteria, as well as yeast, strongly suggests a role for SRCL in host defense (Nakamura et al., 2001a,b).

In the present study, we examined the possible participation of SRCL in the binding and clearance of Aβ in the AD brain. We provide the first evidence that SRCL is expressed, in an Aβ-dependent fashion, in astrocytes, microglia, and vascular/perivascular cells both in a double transgenic mouse model of AD (Tg-APP/PS1) and in cadaveric samples from patients with AD. We further show that SRCL could bind fibrillar $A\beta_{1-42}$ and that its expression was upregulated in the brains of patients with AD. We propose that SRCL may play an important role in Aβ binding, and presumably in clearance, by glial and vascular/perivascular cells in the AD-affected brain, acting in an Aβ dose-dependent manner.

MATERIALS AND METHODS

Animals

Timed pregnant Sprague-Dawley rats and C57/BL6 mice were purchased from SLC (Shizuoka, Japan). Double transgenic mice (Tg-APP/PS1) (Sakaguchi and Kudo, unpublished) and wild-type littermates (WT) were generated by crossing PS1 'knock-in' mice (Nakano et al., 1999) with transgenic mice (Tg2576) that overexpress the Swedish mutation of the human amyloid precursor protein (Hsiao et al., 1996). Animals were housed in individual cages in a temperature-controlled room under a 12-hr light/12-hr dark cycle. Procedures were approved by the Osaka University Graduate School of Medicine Ethics Committee. All efforts were made to minimize animal discomfort and the number of animals used.

Human Materials

Temporal cortex tissues from four cadavers with AD (average age at death = 84.2 ± 2.8) and three non-AD cortex samples (average age at death = 56.7 ± 26.1) were studied. All samples were obtained from the Brain and Tissue Bank of the University of Maryland and handled under procedures approved by the Institutional Review Board for Human Subject Research.

cDNA Cloning of Rat *SRCL* Coiled-Coil Region

Rat *SRCL* coiled-coil region sequence was cloned by PCR from hexaoligonucleotide primed cDNA of rat microglial total RNA by using the following primers: forward (F), 5′-GCAAGCAAATGGGGACTC-3′, corresponding to the putative coiled-coil initiation site of mouse *SRCL ORF* (residue 417), and reverse (R), 5′-AGGTGATGGGCTGTG-TAG-3′ corresponding to the putative coiled-coil ending site of *mSRCL* (residue 1070). PCR products were subcloned into pGEM-T vector (Promega, Madison, WI), and authenticity of the expression vector was confirmed by sequence analysis.

Northern Blot, RT-PCR, and Quantitative Real-Time RT-PCR Analyses

Total RNA was prepared from cells and tissues of adult and postnatal day 7 (P7) rats, as well as from temporal cortex of human autopsy samples, by using an ISOGEN Kit (Nippongene, Japan) or RNeasy Micro Kit (QIAGEN) according to the manufacturer's instructions. For Northern blotting, polyA+ RNA was prepared from total RNA of adult tissues; and 2 μg of polyA+ RNA was electrophoresed in a 1% agarose/0.7% formamide gel, blotted onto a Hybond N+ nylon membrane, and hybridized with ^{32}P-labeled cDNA fragment (nucleotides 493–1146 of human *SRCL*). Subsequently, the filter membrane was washed with high stringency, and visualized as previously described (Nakamura et al., 2001a,b). A rat *GAPDH* probe was used as a loading control.

For reverse transcription-PCR (RT-PCR), total RNA was pretreated with RNase-free DNase (Qiagen) and 1 μg selected RNA was reverse transcribed with SuperScript II (Invitrogen) and primed with random hexamers according to manufacturer's instructions. For rat experiments, after a 5-min denaturation at 95°C, 32 cycles of PCR amplification consisting of 94°C for 1 min, 58°C for 1 min, and 72°C for 1 min, followed by an extension phase of 72°C for 7 min, were carried out by using a GeneAmp Gold PCR Reagent Kit (Perkin-Elmer). The number of amplifications cycles and amount of cDNA used for each reaction were optimized for quantification of RNAs in preliminary experiments. PCR products were resolved by 1.5% agarose gel electrophoresis, and the gel was then stained with ethidium bromide. Rat *SRCL* primers were as follow: rat *SRCL*-forward (F), 5′-TTCTTTCCTCATCACCAC-3′; and rat *SRCL*-reverse (R), 5′-TGTTCACAATATCTGTCTC-3′. For normalization, *GAPDH* mRNA was used. For mouse experiments, the following RT-PCR protocol was used. After a 5-min denaturing incubation at 94°C, 32 cycles of PCR amplification consisting of 94°C for 30 sec, 63°C for 30 sec, and 72°C for 3 min, followed by an extension at 72°C for 5 min, was carried out by using the above reagent kit. Primers for mouse *SRCL* and mouse *GAPDH* were: mouse *SRCL-F*, 5′-ACACTGGTACGACTTCTCCGG-3′; mouse *SRCL-R*, 5′-CATTCTTCGGCTTTCAGAGGC-3′; mouse *GAPDH-F*,

5′-CGTGTTCCTACCCCCAATGT-3′; mouse *GAPDH-R*, 5′- TGTCATCATACTTGGCAGGTTTCT-3′. For real-time quantitative RT-PCR, 2.5 μg of each RNA was reverse transcribed by using SuperScript II (Invitrogen) according to manufacturer's instructions. For human autopsy samples, a High-capacity cDNA Archive Kit (Applied Biosystems, Foster City, CA) was used. Real-time RT-PCR was carried out with an ABI PRISM 7900 sequence detection system (Applied Biosystems) to quantify relative levels of mRNA in samples. For amplification of *hSRCL* and *GAPDH*, as an endogenous control, Universal PCR master mix (Applied Biosystems) and TaqMan MGB probes (FAM dye-labeled) were used for *hSRCL* (exon 5–6, Hs00560477m1; Applied Biosystems) and for human *GAPDH* (TaqMan VIC Probe; 4326317E; Applied Biosystems). All standards and samples were assayed in triplicate. Thermal cycling was initiated with an initial denaturation at 50°C for 2 min and 95°C for 10 min, followed by 40 cycles of PCR (95°C for 15 sec; 60°C for 1 min). Results were expressed as means ± standard error (SE) of the number of observations. Statistical significance was assessed by Student's *t*-test. A level of $P < 0.05$ was considered significant. Significance was determined after two separate experiments.

Cell Line Cultures

Cell lines CHO-K1, C6, J774A.1, and PC12 were cultured as described previously (Funakoshi et al., 1991; Naveilhan et al., 1996; Nakamura et al., 2001a,b).

Microglial Cultures

We prepared primary mixed-glia culture from newborn mice/rats (P1-3), and isolated primary astrocytes and microglia as described previously (Funakoshi et al., 2002). Mouse microglial cells were maintained in Dulbecco's modified Eagle's medium (DMEM) with 10% FBS. Rat microglial cells were maintained in serum-free modified N3, composed of high-glucose DMEM/Ham's F12 (DF) medium containing transferrin, insulin, progesterone, and sodium selenite (Funakoshi et al., 2002). In each primary microglial culture, microglial purity was approximately 95% as judged from Mac-1 (CD11b) immunostaining.

Preparation of Mouse Secondary Astrocytes

Primary astrocytes were prepared from P1 C57/BL6 mice largely as described previously (Funakoshi et al., 2002). Briefly, cerebral cortices were dissected, and the meninges were removed completely. The tissues were then minced, suspended in phosphate-buffered saline (PBS) containing 0.05% trypsin (GIBCO, Grand Island, NY) at 37°C for 10 min, and thereafter incubated with 0.01% DNase I (Sigma, St. Louis, MO) for 5 min at room temperature (RT). After incubation and centrifugation, the cell pellets were washed three times. Cells were filtered through a 75-μm nylon mesh, sedimented by centrifugation, suspended in low glucose DMEM (Nacalai tesque, Kyoto, Japan) containing 10% FBS (JRH Bioscience, Lenexa, KS), 100 IU/ml penicillin and 100 mg/ml streptomycin, and transferred to culture dishes. Once the cells had become confluent, they were rinsed with PBS, suspended in trypsin-containing PBS, and subcultured in DMEM/1% FBS in 6-well plates. After 3 days, the culture plates were rocked vigorously for 2 hr at RT to remove microglia. Astrocyte purity was >95% after 3 days in culture as judged from double immunostaining with anti-GFAP (Chemicon International, Temecula, CA) and anti-ionized calcium-binding adapter molecule-1 (Iba1) antibody (Wako Pure Chemical, Osaka, Japan).

fAβ Binding and Competition Assays

Human $fA\beta_{1-42}$ peptide (Seikagaku Kougyou, Tokyo, Japan) was dissolved in DMSO and diluted in sterile water to 1 mg/ml according to the manufacturer's instructions, and fibrillated just before usage. Twenty-four hours after isolation from primary mixed glial cultures, mouse microglial cells were treated at 37°C for 1 hr with 2.5 μg/ml $fA\beta_{1-42}$ in DMEM supplemented with 10% FBS. The cells were washed extensively with ice-cold PBS, fixed with 4% paraformaldehyde (PFA) in PBS, incubated with primary antibodies anti-CD11b (Mac-1) and anti-Aβ (6E10), followed by Alexa546 (red)- and Alexa488 (green)-conjugated secondary antibodies, counterstained with Hoechst 33342 (Molecular Probes), and observed under a LSM510 confocal microscope. Twenty-four hours after transfection with h*SRCL-I*, *-II*, m*SR-AI-Myc* or *Mock*-expression vector, CHO-K1 cells were treated at 37°C for 30 min with 2.5 mg/ml $fA\beta_{1-42}$ with or without 500 μg/ml Fucoidan, 200 μg/ml poly(C), or 200 μg/ml poly(G) in Ham's F12 medium supplemented with 10% FBS. The cells were visualized with anti-Myc (12A5) and anti- fAβ antibody as described above.

fAβ Treatment of Primary Mouse Astrocytes

Human $fA\beta_{1-42}$ peptide was dissolved in DMSO and diluted in PBS to 300 mM, corresponding to 1.35 mg/ml, and incubated for 3 days at 37°C, and subsequently sonicated when required, to prepare fAβ.

Preparation of Antibody

The synthetic peptide QPD (KAGQPDNWGHGHGP-GEDC) (Nakamura et al., 2001a), corresponding to a part of the CRD region of the hSRCL, was obtained from MBL (Osaka, Japan) (Fig. 4A). Rabbits were immunized with the QPD peptide coupled to keyhole limpet hemocyanin (KLH) by M-maleimidobenzol-*N*-hydroxysuccinimide ester. The antiserum was purified on an affinity column of CNBr-activated Sepharose4B (Amersham) coupled to the immunogen without KLH and referred to here as anti-SRCL antibody (OT667).

Western Blot Analysis

Twenty-four hours after transfection with the desired constructs, CHO-K1 cells and J774A.1 cells were lysed. The lysates were electrophoresed under reducing conditions, and then immunoblotted with anti-SRCL antibody. An ECL system was used for visualization.

Immunohistochemistry

Mice were deeply anesthetized and transcardially perfused with cold PBS followed by cold 4% PFA in PBS. The brains were removed and postfixed for 1.5 hr at 4°C and separated at the midline into halves. One half was immersed in a series of sucrose (10%, 20%) in PBS and frozen in CO_2 gas to prepare frozen sections. The other half was dehydrated and embedded in paraffin according to standard procedures and cut into sections. For human materials, 10% formalin-fixed brain tissues were embedded in paraffin and cut into sections. Paraffin sections were deparaffinized and rehydrated by sequential 5-min incubation in 100%, 95%, and 75% ethanol. The sections were then rinsed twice in water and twice in PBS. Endogenous peroxidase activity was quenched by incubation for 5 min with 3% H_2O_2. To unmask antigens, we immersed the slides for 10 min at RT in 50 mM Tris-HCl (pH 8.0) containing 0.4 mg/ml Proteinase K and then washed them in PBS. Sections were blocked for 30 min at RT with blocking buffer consisting of 5% normal goat serum and 0.3% Triton X-100 in PBS. For Aβ immunostaining, sections were pre-treated with 70% formic acid for 1 min, blocked with blocking buffer and incubated with primary antibodies for 1.5 hr at RT. The following antibodies were used: affinity-purified rabbit anti-SRCL (OT667, 3 mg/ml), mouse anti-GFAP (1:400; MAB3402; Chemicon, for astrocytes), rat anti-Mac-1 (1:100; Chemicon;, for microglia and macrophage including MATO cells), rabbit anti-Iba-1 (1:1,000; WAKO, Japan;, for microglia and macrophages including MATO cells), mouse anti-rat CD-31 (1:200; PECAM-1; Pharmingen; activated, Lewis rat-derived microglia as immunogen, for activated microglia/macrophages, MATO and endothelial cells), anti-αSMA (1:500; DAKO; for smooth muscle cells), and rabbit anti-Aβ40 (1:1,500; FCA3340) and rabbit anti-Aβ42 (1:1,500; FCA3542) antibodies (FCA3340 and FCA3542 were kindly provided by Dr. F. Checler). After having been washed three times with PBS, the sections were incubated for 20 min at RT with secondary antibodies conjugated with Alexa488 (green) or Alexa546 (red), and subsequently washed with PBS and mounted.

Human tissue sections were visualized as brown signals by incubation with the EnVision+ System (K4001 for mouse/K4003 for rabbit; Dako, Glostrup, Denmark) and 3,3′-diaminobenzidine tetrahydrochloride (DAB; Wako, Japan) as the chromogen. For double labeling immunohistochemistry, after visualization of the first primary antibody with DAB, sections were microwaved for 5 min in citrate buffer (pH 6.0), and then were washed and incubated with the second primary antibody. Samples were visualized as pink signals by using an alkaline phosphatase-conjugated anti-rabbit IgG (Vector, CA) and a Vector Red Alkaline Phosphatase Substrate Kit according to the manufacturer's instructions, and counterstained with Mayer's hematoxylin (WAKO). For preabsorption, some sections were incubated with anti-SRCL antibody that had been pre-absorbed with an excess amount of immunogen. For double immunostaining of $A\beta_{1-40}/A\beta_{1-42}$ and SRCL, rabbit anti-$A\beta_{1-40}/A\beta_{1-42}$ antibodies and affinity-purified rabbit anti-SRCL antibody were labeled with Alexa546 and Alexa488, respectively, by using a Zenon Alexa Fluor Rabbit IgG Labeling Kit (Molecular Probes) according to the manufacturer's instructions and used for direct immunofluorescence staining.

RESULTS

cDNA Cloning of Rat *SRCL* Coiled-Coil Region

We first wished to compare the sequence of the region of rat *SRCL* cDNA encoding the coiled-coil domain with human and mouse sequences. We carried out RT-PCR using cDNA generated from rat microglial cells amplified with primers based on mouse *SRCL* cDNA. The cloned cDNA corresponding to the rat *SRCL* coiled-coil domain was highly similar to that of human and mouse *SRCLs*, with 88% and 95% identity, respectively, at the nucleotides level, 91.7% and 95.9% identity, respectively, at the amino acid level, and containing 8 putative *N*-glycosylation sites. This degree of conservation suggests that the glycosylation sites are important for folding, maturation, or function of the SRCL protein.

Rat *SRCL* mRNA Is Expressed in Various Tissues as a Single Transcript

Human *SRCL* is transcribed as 2 different isoforms, i.e., human *SRCL* type I (h*SRCL-I*) and *SRCL* type II (h*SRCL-II*). *hSRCL-I*, containing a C-type CRD, is the major transcript found in human tissues; and it is resolved as a 3.0-kb species by Northern blotting. In contrast, h*SRCL-II*, which lacks the C-type CRD, exhibits a 4.5-kb species on Northern blots. Mouse *SRCL* is resolved as a single 3.0-kb transcript corresponding to h*SRCL-I*; and no other transcripts are seen, suggesting that mice express only one isoform. We examined various rat tissues for expression of *SRCL* isoforms using Northern blotting. *SRCL* mRNA was widely expressed in them. Using a probe targeting the coiled-coil region of rat *SRCL*, we found its mRNA to be resolved as a single 3.0-kb band (Fig. 1). Expression was highest in the lung, followed by the spleen, small and large intestine, stomach, and brain; whereas rat *SRCL* mRNA expression was below detection limits in the liver. Thus, like mice, rats expressed only one *SRCL* transcript, which corresponded to h*SRCL-I*.

Rodent Microglia and Astrocytes Express *SRCL* mRNA

It has been suggested that microglia and astrocytes in the brains of patients with AD are associated with senile plaques and contribute to recognition, ingestion, and elimination of fibrillar β-amyloid peptide (fAβ) from plaques. This could be facilitated by scavenger receptors on the cell surface. To determine whether these cells express SRCL, we examined *SRCL* mRNA expression in cultured rodent microglia (Fig. 2A,B) and astrocytes by using semiquantitative RT-PCR. After a 24-hr culture period (1 day in vitro, 1DIV), *SRCL* mRNA was detected in astrocytes (ASTRO) and at 2DIV in microglia (MG, 2-day culture; Fig. 2C). In contrast, *SRCL* mRNA expression was below the detection limit in neurons (PC12 cells) and C6 glioma cells (Fig. 2C). These findings show that *SRCL* mRNA was primarily expressed in glial cells but not in neurons among neural

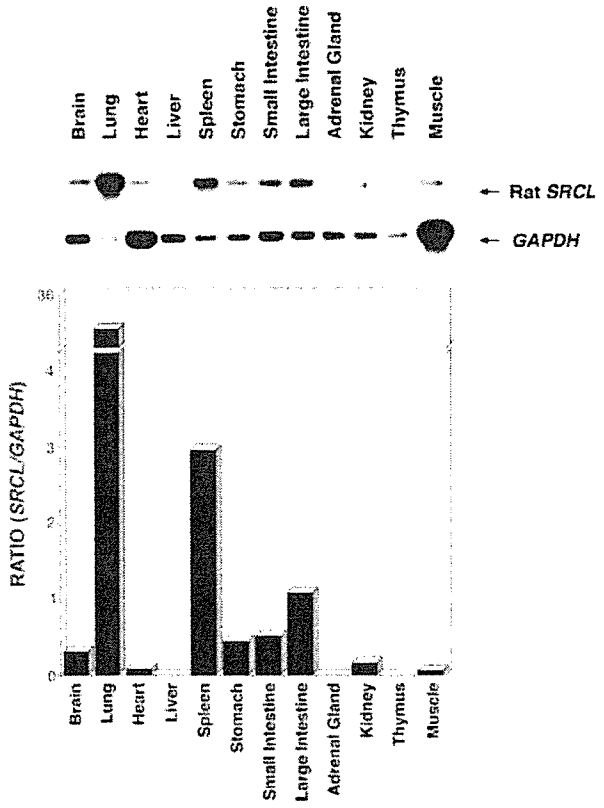

Fig. 1. Northern blot analysis of rat *SRCL* mRNA in various adult rat tissues. **Upper panel:** rat *SRCL* is widely expressed as a single 3.0-kb transcript. Highest expression of mRNA was detected in lung followed by spleen, intestine, stomach, and brain. *GAPDH* served as a loading control. **Lower panel:** level of *SRCL* mRNA relative to *GAPDH* mRNA is presented based on the densitometry analysis.

cells in vitro. In addition, we found that the level of *SRCL* mRNA increased in a culture time-dependent manner (MG) or was regulated by the application of amyloid-β peptide (ASTRO). In microglia, *SRCL* mRNA expression levels increased during the culture time, and the level at 2 days of culture was higher than that in the brain (Br) at postnatal day 7 (P7; Fig. 2D); i.e., the level increased at 2 days of culture when the cultured microglia showed activated morphology as compared to that at 1 day (Fig. 2B,A, respectively). It seems likely that the level of *SRCL* mRNA in microglia is correlated with the state of microglial activation. To determine whether $fA\beta_{1-42}$ could alter the expression of *SRCL* mRNA, we treated cultured mouse neonatal astrocytes with $fA\beta_{1-42}$ for the times indicated in Figure 2E, and analyzed expression of *SRCL* mRNA. Using semiquantitative RT-PCR, we observed that the *SRCL* mRNA level increased at 48 hr after $fA\beta_{1-42}$ treatment relative to that of the matched control astrocytes (Fig. 2E). Similar results were obtained when the other primer set for *SRCL* mRNA was used (data not shown).

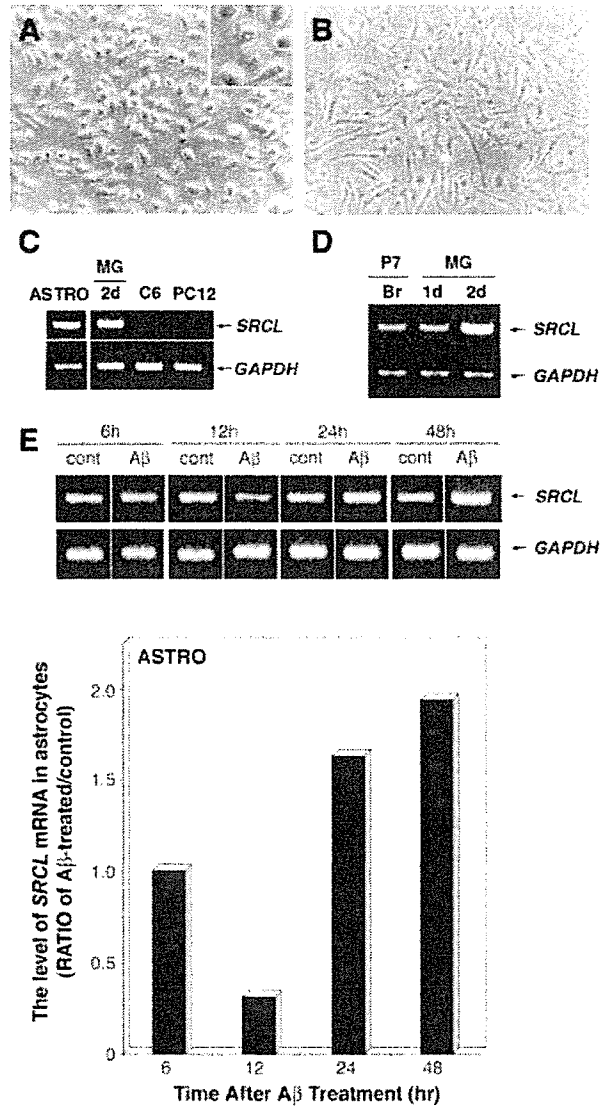

Fig. 2. RT-PCR analysis of *SRCL* mRNA in cultured neonatal microglia and astrocytes. **A,B:** Representative photomicrographs of rat neonatal microglia (MG) after 15 min (A inset, high-magnification view) and 2 days in primary culture (B). **C:** RT-PCR of cultured neural cells: mouse neonatal astrocytes (ASTRO), rat neonatal microglia (MG), human C6 glioma (C6) and rat pheochromocytoma PC12. RT-PCR showed that *SRCL* mRNA expression is prominent in ASTRO and MG, but under the detection limits in C6 and PC12. **D:** RT-PCR of rat *SRCL* mRNA in cultured neonatal microglia at different times after the start of the culture. The level of *SRCL* mRNA was increased at 2 days after the start of the culture (2d) compared to that at 1 day (1d) and the former level became higher than postnatal day 7 (P7) brain (Br). **E:** RT-PCR of cultured astrocytes treated with $fA\beta_{1-42}$. The level of *SRCL* mRNA in astrocytes was increased at 48 hr after $fA\beta_{1-42}$ application. *GAPDH* served as a loading control. The ratio of rat *SRCL* mRNA levels (Aβ-induced level vs. matched control level) is expressed in the lower panel.

The induction levels of *SRCL* mRNA in microglia were almost comparable to that of astrocytes in vitro (1.9 vs. 2.4). Taken together with our previous finding that SRCL acts as a scavenger receptor (Nakamura et al., 2001a,b), these results suggest that SRCL-expressing activated glial-cells may recognize a variety of substances in neurodegenerative tissues, such as fAβ in the AD-affected brain.

Mouse Primary Microglia Bind and Ingest Synthetic $fA\beta_{1-42}$ Microaggregates

To determine the role of SRCL expressed in activated glial cells in the recognition of $fA\beta_{1-42}$, we developed positive-control conditions in which fibrillar $A\beta_{1-42}$ was recognized and ingested by primary microglia. When we incubated primary microglia for 1 hr with $fA\beta_{1-42}$ prepared from synthetic $A\beta_{1-42}$ peptides by a 3-day incubation at 37°C, we observed a high degree of cellular binding and ingestion of $fA\beta_{1-42}$ microaggregates (Supplementary Fig. 1).

Human SRCL-I and SRCL-II Expressed in CHO-K1 Cells Bind $fA\beta_{1-42}$

To investigate whether SRCL would have the ability to bind $fA\beta_{1-42}$, we examined $fA\beta_{1-42}$ binding by CHO-K1 cells transiently expressing hSRCL-I in the presence or absence of Fucoidan, one of the major ligands for scavenger receptors (SRs). CHO-K1 cells expressing mouse Class A Type I scavenger receptor (mSR-AI) served as a positive control for the assay. CHO-K1 cells transiently transfected with m*SR-AI-Myc* or h*SRCL-I-Myc* were incubated with $fA\beta_{1-42}$ for 1 hr at 37°C. After extensive washing with PBS, the cells were fixed and processed for immunostaining with antibodies against $fA\beta_{1-42}$ and Myc to visualize mSR-AI-Myc or hSRCL-I-Myc. The $fA\beta_{1-42}$ binding (green color) was specifically seen in CHO-K1 cells expressing mSR-AI-Myc or hSRCL-I-Myc (red color), whereas the binding was markedly competed in the presence of an excess amount of Fucoidan (Fig. 3A). To further confirm the ability of SRCL to bind $fA\beta_{1-42}$, we generated CHO-K1 cells stably expressing m*SRCL-Flag* (*Flag-tag* was fused to the cytosolic end of m*SRCL*). A similar result was obtained when Cy3-labeled-$fA\beta_{1-42}$ (Cy3-$fA\beta_{1-42}$) binding to CHO-K1 cells stably expressing mSRCL was examined (Supplementary Fig. 2). In contrast to the failure of the parental CHO-K1 cells to bind Cy3-$fA\beta_{1-42}$, CHO-K1 cells stably expressing mSRCL showed strong binding capacity for Cy3-$fA\beta_{1-42}$ (red color), and this binding was competed by Fucoidan (Supplementary Fig. 2). These findings show that SRCL specifically bound to $fA\beta_{1-42}$ by using the same residues interacting with other scavenger receptor ligands, such as Fucoidan.

To further investigate whether the CRD region of SRCL would be essential for the binding of $fA\beta_{1-42}$ to SRCL, we examined $fA\beta_{1-42}$ binding to CHO-K1 cells transfected with m*SR-AI-Myc*-, h*SRCL-I-Myc*, h*SRCL-II-Myc*-, or *Mock*-expression vectors. Interestingly, in addition to CHO-K1 cells expressing mSR-AI, those cells expressing either isoform of hSRCL efficiently bound $fA\beta_{1-42}$, but *Mock*-transfected cells did not (Fig. 3B). Given the differences in domain composition between hSRCL-I and -II, it seems that $A\beta_{1-42}$ binding was primarily mediated by SRCL collagenous domains and that the CRD of hSRCL-I contributed relatively little to the binding. Finally, we examined $fA\beta_{1-42}$ binding to these cells in the presence of polyguanylic acid (poly(G)), a ligand for scavenger receptors that inhibits $fA\beta_{1-42}$ binding to the polycationic region of the collagenous domain of SR-AI. Poly(C) served as a negative control. The binding of $fA\beta_{1-42}$ to CHO-K1 cells expressing mSR-AI was not inhibited by 200 μg/ml poly(C) but was inhibited by 200 μg/ml poly(G). To see whether hSRCL binding to $fA\beta_{1-42}$ was mechanistically similar to binding by mSR-AI, we carried out the same assay with cells expressing hSRCL-I or -II. In contrast to the results for mSR-AI, the binding of $fA\beta_{1-42}$ by cells expressing either isoform was not sensitive to poly(G) (200 μg/ml; Fig. 3B). Although we cannot exclude the possibility that hSRCL-I and -II bind to $fA\beta_{1-42}$ differently than does mSR-AI, we consider the most likely explanation for this difference to be the larger number of polycationic regions in the collagenous domain of SRCL (three domains) versus the single domain in SR-AI and thus it seems likely that the binding affinity of SRCLs to $fA\beta_{1-42}$ might be higher than that of SR-AI, as seen in the Poly(G) competition assay.

Immunohistochemical Localization of Mouse SRCL in Tg-APP/PS1

For immunolocalization of SRCL protein in AD-affected brains, we generated a rabbit anti-hSRCL polyclonal antiserum specific for the QPD sequence of the CRD region of hSRCL (Nakamura et al., 2001a,b). The antiserum was purified by using an affinity column bearing the immunized peptide and the resultant purified antibody is referred to hereafter as anti-SRCL antibody. Because hSRCL-I and mSRCL but not hSRCL-II have the CRD region containing the QPD sequence, this anti-SRCL antibody was expected to recognize specifically hSRCL-I and mSRCL (Fig. 4A).

Western blot analysis using the anti-SRCL antibody showed that this antibody recognized the SRCL protein in human *SRCL-I-Myc/EGFP*-transfected cells (h*SRCL-I-Myc/EGFP*), mouse *SRCL-Myc/EGFP*-transfected cells (m*SRCL-Myc/EGFP*), and J774A.1 mouse macrophage at the expected molecular size but not that in *Mock/EGFP*-transfected cells or h*SRCL-II-Myc/EGFP*-transfected cells (Fig. 4B). The small differences seen in the molecular weight of the reactive proteins may reflect differences in glycosylation patterns. To further confirm the specificity of this antibody, we immunostained *hSRCL-I-Myc/EGFP*-, h*SRCL-I-Myc/EGFP*- and *mSRCL-Myc/EGFP*-transfected CHO-K1 cells with anti-SRCL antibody. Immunostaining of the transfected

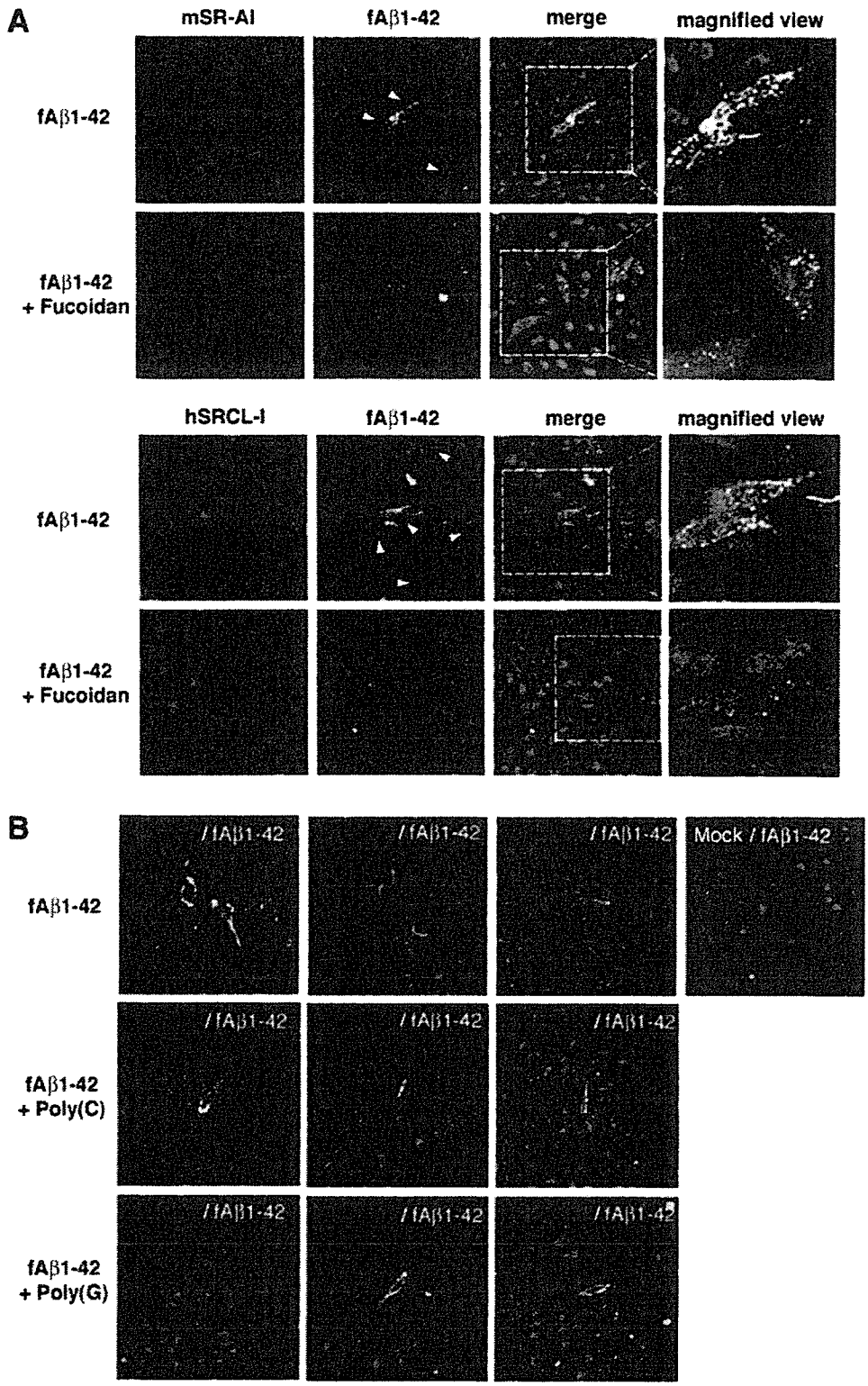
A
mSR-AI
fAβ1-42
merge
magnified view
fAβ1-42
fAβ1-42
+ Fucoidan
hSRCL-I
fAβ1-42
merge
magnified view
fAβ1-42
fAβ1-42
+ Fucoidan
B
/ fAβ1-42
Mock / fAβ1-42
fAβ1-42
fAβ1-42
+ Poly(C)
fAβ1-42
+ Poly(G)

Figure 3.

cells showed that this antibody recognized CHO-K1 cells transiently expressing hSRCL-I-Myc/EGFP or mSRCL-Myc/EGFP but did not recognize CHO-K1 cells expressing Mock/EGFP or hSRCL-II-Myc/EGFP (Fig. 4C). In addition, preabsorption of anti-SRCL antibody with immunogen eliminated the ability of this antibody to recognize CHO-K1 cells expressing hSRCL-I-Myc/EGFP (Fig. 4C). These observations clearly show the specificity of the anti-SRCL antibody for hSRCL-I and mSRCL.

Using this antibody, we examined the immunolocalization of SRCL in Tg-APP/PS1, a double transgenic mouse model of familial AD that coexpresses a mutated amyloid-beta precursor protein and a mutated form of human presenilin-1. In wild-type littermates, we observed no specific SRCL-immunoreactivity (IR) in microglia and astrocytes located in the cerebral cortex (Fig. 5A,B, upper panel, arrow), except for the specific staining for SRCL in perivascular macrophages (MATO cells; data not shown; Fig. 6C, arrowheads). In contrast, a large amount of SRCL-IR was visualized in GFAP-positive, plaques-surrounding reactive astrocytes in both cerebral cortex and hippocampus of 9-month-old Tg-APP/PS1 (Fig. 5A). The intensity of SRCL-IR was strong in GFAP-positive astrocytes situated close to Aβ plaques (Fig. 5A, arrowheads), but weak in those located far away from such Aβ plaques (Fig. 5A, arrows). These data are consistent with our finding that Aβ increased SRCL level in astrocytes in vitro (Fig. 2E). In contrast, SRCL-IR was not detected in wild-type mice and was only weakly present in neurons in amyloid CA1 regions of the hippocampus in association with Aβ-plaque in 9-month-old Tg-APP/PS1 (Fig. 5A, lowest panel). In microglia, SRCL-IR was under the detection limit in wild-type mice (Fig. 5B, upper panel); whereas slight upregulation of SRCL-IR in microglia was seen in association with Aβ plaques in Tg-APP/PS1 in vivo (Fig. 5B, lower panel, arrowhead). These findings suggest that SRCL would play an important role in glial cells such as astrocytes and microglia in AD.

Next we examined whether SRCL could be induced in cells after the development of cerebral amyloid angiopathy (CAA), a typical pathologic feature in AD, by double-immunostaining for SRCL and $A\beta_{1-42}$ or $A\beta_{1-40}$ in the cerebral cortex of 9-month-old Tg-APP/PS1 mice and their wild-type littermates. In age-matched wild-type littermates, no specific staining for Aβ-IR or SRCL-IR was seen inside the leptomeningeal vessel (m.v.; Fig. 6A, upper panel, arrowhead), except for the specific staining for SRCL in perivascular macrophages (MATO cells; data not shown). In contrast, colocalization of SRCL-IR and $A\beta_{1-42/1-40}$ was evident specifically in leptomeningeal vessels showing characteristics of CAA in Tg-APP/PS1 mice (Fig. 6A, arrows). At high magnification, SRCL-IR and $A\beta_{1-40}$-IR appeared as particles; many were colocalized inside the vessel wall, suggesting the possibility of internalization of Aβ by SRCL on vascular/perivascular cells (Fig. 6A, inset). Sections incubated without first antibody eliminated this staining, confirming the specificity of the SRCL-IR (Fig. 6A, lowest panel).

Figure 6B shows a schematic representation of the vascular/perivascular cells in leptomeningeal vessel (m.v.) of wild-type mice and Tg-APP/PS1. In wild-type mice, the m.v. contains endothelial cells (ECs: light green) that are surrounded by smooth muscle cells (SMCs: orange), and its vessel wall is thin. Beside the vessel, perivascular macrophage (MATO cell: yellow) is present. In the m.v. of Tg-APP/PS1, a large amount of Aβ (red) is localized within the vascular wall. Many macrophages (MO: yellow) having attached to the outer surface of and infiltrated into the vascular wall, the number of SMCs has increased and the vessel wall becomes thicker during the progression of disease. It is of note that the vascular/perivascular cells contain multiple Aβ particles (red) inside the cells, possibly as a result of ingestion. These Aβ-containing cells include not only macrophage (MO) and MATO cells, but also SMCs and ECs. Despite the knowledge of Aβ localization, the molecules responsible for Aβ binding and ingestion are not well defined.

Because SRCL-IR was colocalized with $fA\beta_{1-40/1-42}$-IR within Tg-APP/PS1-vessels (Fig. 6A), we next assessed which vascular/perivascular cells expressed SRCL by using vascular/perivascular cell-specific antibodies: anti-rat CD31 (activated Lewis rat microglia as immunogen, a marker for microglia/macrophage including MATO cells and ECs), anti-αSMA (for SMCs), and anti-GFAP antibody (for astrocytes). In wild-type littermates, we did not easily observe SRCL-IR (green) co-present with CD31-IR (red; Fig. 6C. upper panel), except for MATO cells (Fig. 6C, arrowheads). SRCL-IR was only weakly detected in αSMA-positive SMCs and fairly well detected in CD31-positive ECs in the m.v. of wild-type littermates (Fig. 6C, middle and upper panels, respectively). In contrast to wild-type littermates, we could detect strong SRCL-IR (green) in subpopula-

Fig. 3. Binding of synthetic fibrillar $A\beta_{1-42}$ to CHO-K1 cells expressing *hSRCL-I* or *-II* and competition by poly(G). **A:** hSRCL-I mediates $fA\beta_{1-42}$ binding to CHO-K1 cells, and the binding is eliminated by Fucoidan. m*SR-AI-Myc*,- or h*SRCL-I-Myc*-transfected-CHO-K1 cells treated with $fA\beta_{1-42}$ were visualized with anti-Myc and anti-Aβ antibodies followed by Alexa546 (red)- and Alexa488 (green)-conjugated antibodies, respectively. Synthetic $fA\beta_{1-42}$ microaggregates (green) specifically bound to m*SR-AI-Myc*- and h*SRCL-I-Myc*-expressing cells (red). Nuclei (in blue) were counterstained with Hoechist33342. **B:** Competition assays with poly(C) or poly(G). m*SR-AI-Myc*-, h*SRCL-I-Myc*-, h*SRCL-II-Myc*- or *Mock*-transfected CHO-K1 cells were incubated with PBS containing $fA\beta_{1-42}$ and an excess amount of poly(C) or poly(G), and the cells were then visualized with anti-Myc and anti-Aβ antibodies detected with Alexa546 (red)- and Alexa488 (green)-conjugated antibodies, respectively. Synthetic $fA\beta_{1-42}$ microaggregates (green) specifically bound to m*SR-AI-Myc*- h*SRCL-I-Myc*-, and h*SRCL-II-Myc*-expressing cells (red), but not to mock-transfected cells. Poly(G) (200 μg/ml) but not poly(C) (200 μg/ml) could efficiently compete the binding of $fA\beta_{1-42}$ to cells expressing m*SR-AI*, whereas neither poly(G) nor poly(C) could efficiently compete that to cells expressing h*SRCL-I* or h*SRCL-II*.

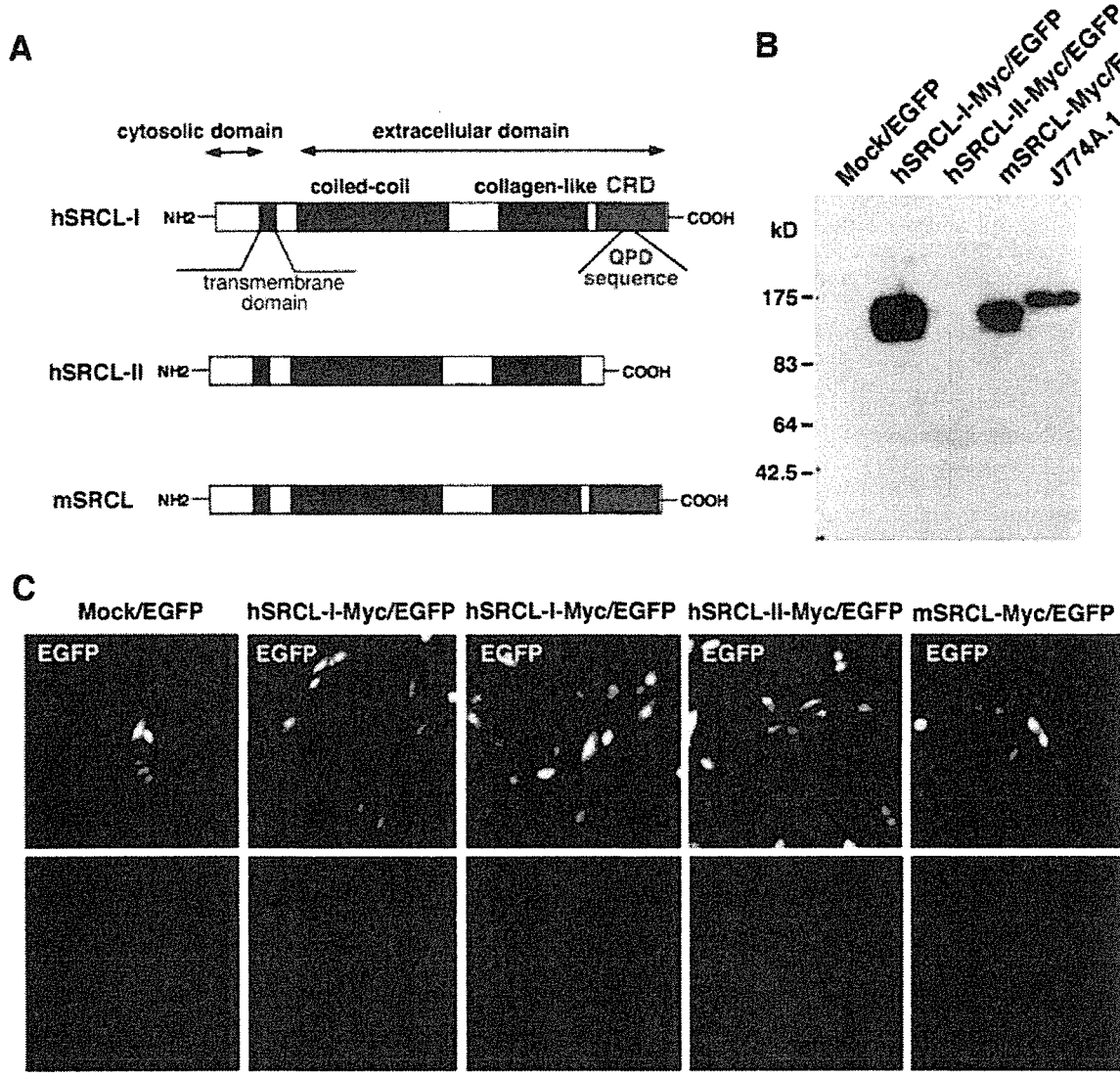

Fig. 4. Western blotting and immunocytochemistry with anti-hSRCL antibody. **A:** Schematic representation of the domain structure of hSRCL-I, hSRCL-II and mSRCL showing the position used as the immunogen for anti-SRCL antibody. CRD, carbohydrate recognition domain. Anti-SRCL serum was raised against the peptide containing the QPD sequence at the CRD of hSRCL, purified by using an affinity column of immunogen; and referred to as anti-SRCL antibody. **B:** Western blotting. CHO-K1 cells were transiently transfected with expression vectors for hSRCL-I-Myc/EGFP, hSRCL-II-Myc/EGFP, mSRCL-Myc/EGFP, and Mock/EGFP. Equal amounts of extracts from the cells were loaded for SDS-PAGE. Western blot analysis was carried out by using the anti-SRCL antibody. J774A.1 cells, a mouse macrophage cell line. **C:** Immunocytochemistry. CHO-K1 cells were transiently transfected with the indicated expression vectors. Two days after the transfection, the cells were fixed in 4% PFA in PBS and immunostained with anti-SRCL antibody and subsequently with Alexa546-conjugated secondary antibody (red), with or without preabsorption of the primary antibody with an excess amount of immunogen.

tions of vascular/perivascular cells of Tg-APP/PS1 mice (Fig. 6D,E). In Tg-APP/PS1, in addition to CD31-IR along with SRCL-IR in MATO cells, SRCL-IR became intense inside the meningeal vascular wall in which infiltrating macrophages had accumulated and in ECs (Fig. 6C, upper panel. arrows; red), suggesting induction of SRCL in macrophages. At high-magnification (Fig. 6D, upper panel), SRCL-IR (green) appeared as multiple particles inside CD31-positive macrophages (red) that had accumulated within the vessel wall, indicating internalization of SRCL by macrophages. SRCL-IR intensity (green) was markedly increased in αSMA-

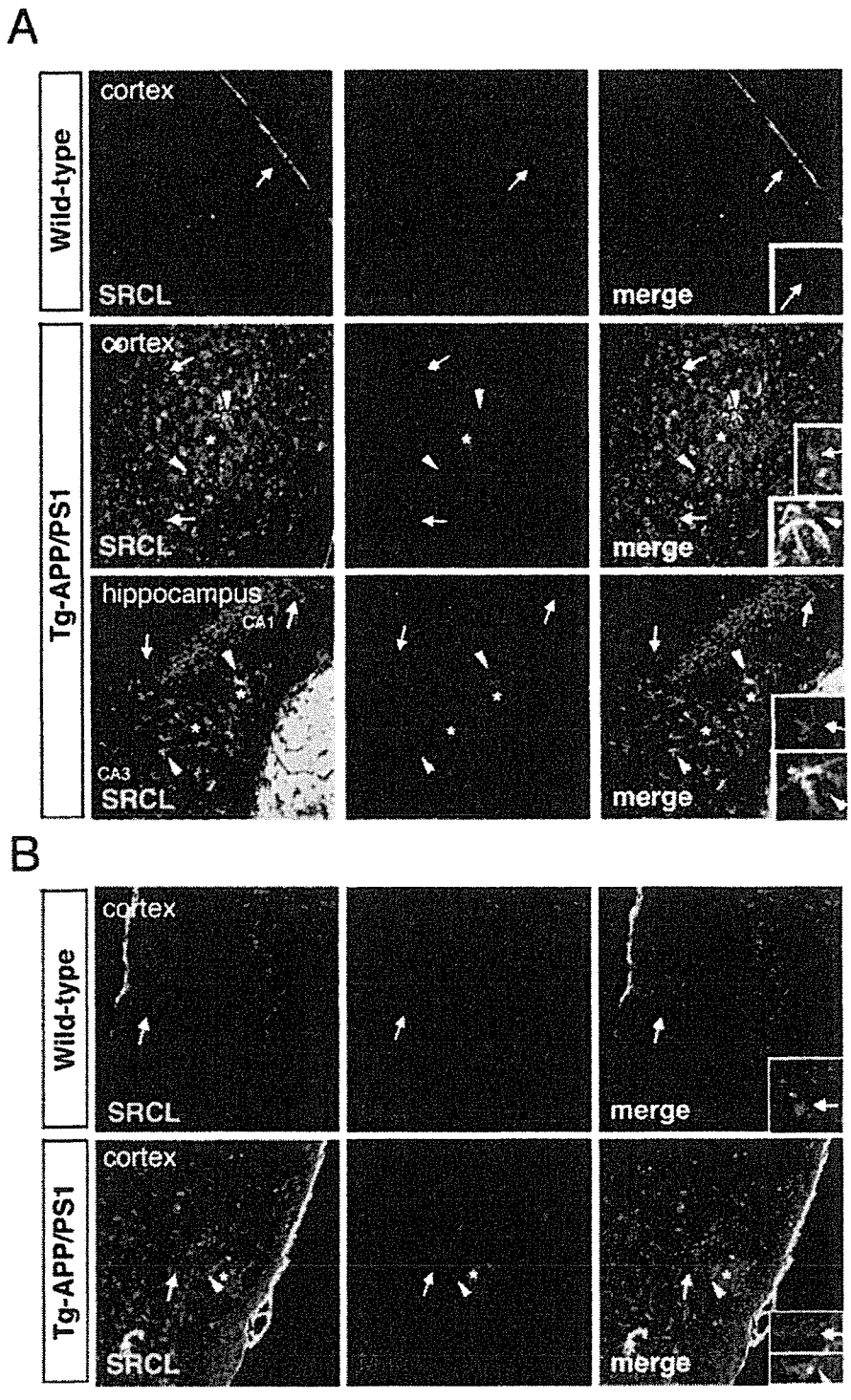

Fig. 5. Immunolocalization of SRCL in cerebral cortex and hippocampus of Tg-APP/PS1 mice and wild-type littermates. **A:** Paraffin sections from 9-month-old Tg-APP/PS1 mice and wild-type littermates were incubated with anti-SRCL and anti-GFAP primary antibodies, followed by their respective Alexa488 (green)- and Alexa546 (red)-conjugated secondary antibodies. Arrows point to cells immunopositive for GFAP only; and arrowheads, to those immunopositive for both SRCL and GFAP. CA1 and CA3 regions of the hippocampus are indicated. **B:** Frozen sections from cortex of a 9-month-old Tg-APP/PS1 and wild-type littermate were incubated with anti-SRCL and anti-Mac-1 primary antibodies, followed by their respective Alexa488 (green)- and Alexa546 (red)-conjugated secondary antibodies. Insets and asterisks in (A) and (B) show high-magnification views and Aβ plaques, respectively. GFAP, astrocytic marker; Mac-1, microglial marker. Arrows point to cells immunopositive for Mac-1 only; and arrowheads to cells immunopositive for both SRCL and Mac-1.

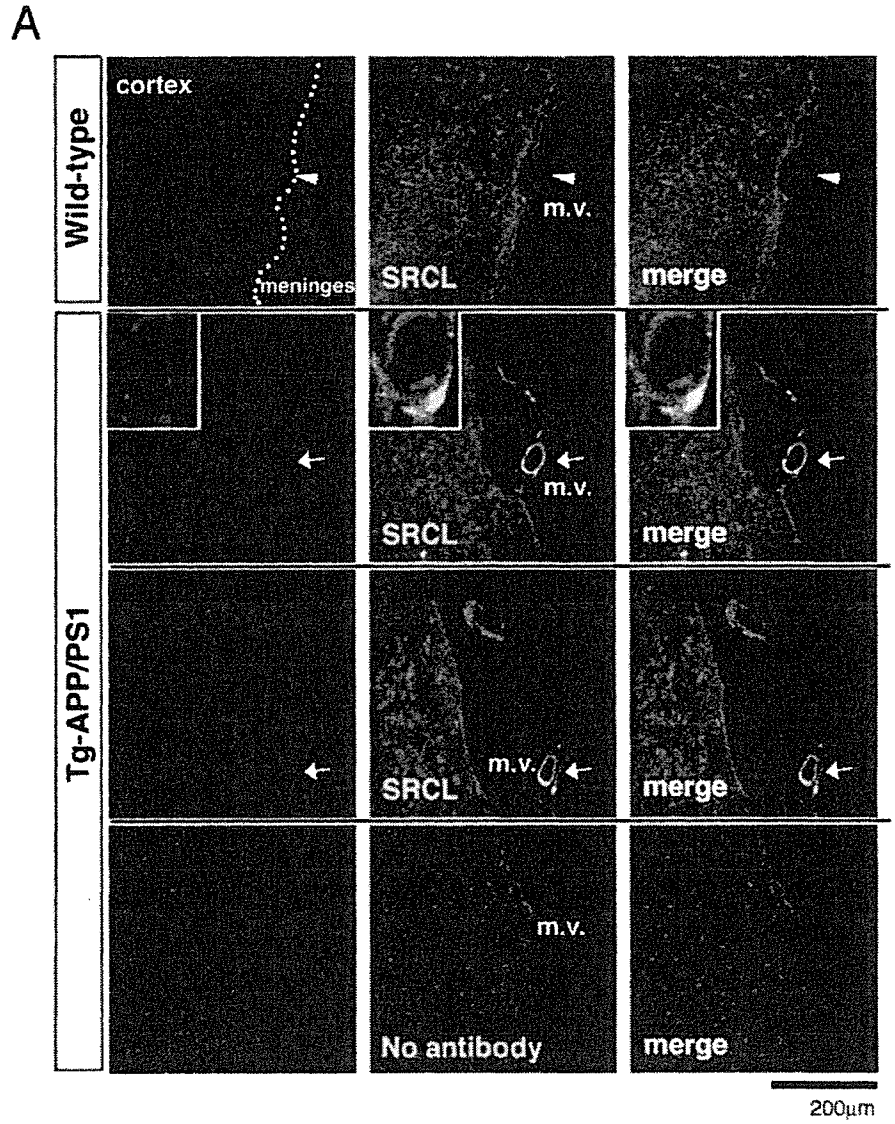

Fig. 6. Immunolocalization of SRCL in cortical vessels of Tg-APP/PS1 mice and wild-type littermates. **A:** Double-immunostaining for SRCL and Aβ in leptomeningeal vessels. Paraffin sections from the cortices of 9-month-old Tg-APP/PS1 mice and wild-type littermates were incubated with rabbit anti-$A\beta_{1-40/1-42}$ and rabbit anti-SRCL antibodies, pre-labeled with Alexa546 (red) and Alexa488 (green), respectively, by using a Zenon rabbit IgG Labeling Kit (Invitrogen), respectively, and counterstained with Hoechst33342 (blue) to visualize nuclei. Arrowheads indicate a meningeal vessel without Aβ-IR or SRCL-IR. Arrows indicate Aβ/SRCL-double positive vessels. Inset, a high-magnification view. Lowest panel represents control immunostaining without anti-SRCL antibody. m.v., meningeal vessel (leptomeningeal vessel). **B:** Schematic representation showing vascular/perivascular cells of leptomeningeal vessels (m.v.). In wild-type mice, thin ECs and SMCs are seen. Beside the vessel, a perivascular macrophage (MATO cell) is seen. In Tg-APP/PS1, thickness of the vessel has increased, and the number of SMCs has increased and many macrophages has infiltrated into the vascular wall. Red color shows the Aβ aggregates in the extracellular matrix and the Aβ particles ingested by the cells. MATO, MATO cell (perivascular macrophage, yellow); SMC, smooth muscle cell (orange); EC, endothelial cell (light green); MO, macrophages (yellow). **C:** Representative pictures of double-immunostaining for SRCL and CD31, αSMA or GFAP in leptomeningeal vessels. Paraffin sections from cortices of 9-month-old Tg-APP/PS1 mice and wild-type littermates were immunostained with anti-SRCL and anti-rat CD31 (for activated microglia/macrophage including MATO cells and ECs; Lewis rat activated microglia as immunogen), anti-GFAP (for astrocytes) or anti-αSMA (for SMCs) as primary antibody, followed by their respective Alexa488 (green)- and Alexa546 (red)-conjugated secondary antibodies. Sections were counterstained with Hoechst33342 (blue). m.v., leptomeningeal vessel. Arrows indicate CD31-positive ECs. **D:** Magnified views of double-immunostaining for SRCL and CD31 or αSMA of leptomeningeal vessels in 9-month-old Tg-APP/PS. Paraffin sections were processed for immunostaining with anti-SRCL, CD31 or αSMA as described above. **E:** Representative photo of double-immunostaining for SRCL and GFAP in cortical tissues associated with amyloid plaques (asterisks) and cortical amyloid angiopathy in a 9-month-old Tg-APP/PS1. Paraffin sections were processed for immunostaining using anti-GFAP and anti-SRCL primary antibodies, followed by their respective Alexa546 (red)- and Alexa488 (green)-conjugated secondary antibodies. Intra-cortical vessel is indicated as "c.v." at the right bottom corner of the merged view. Asterisks indicate amyloid plaques.

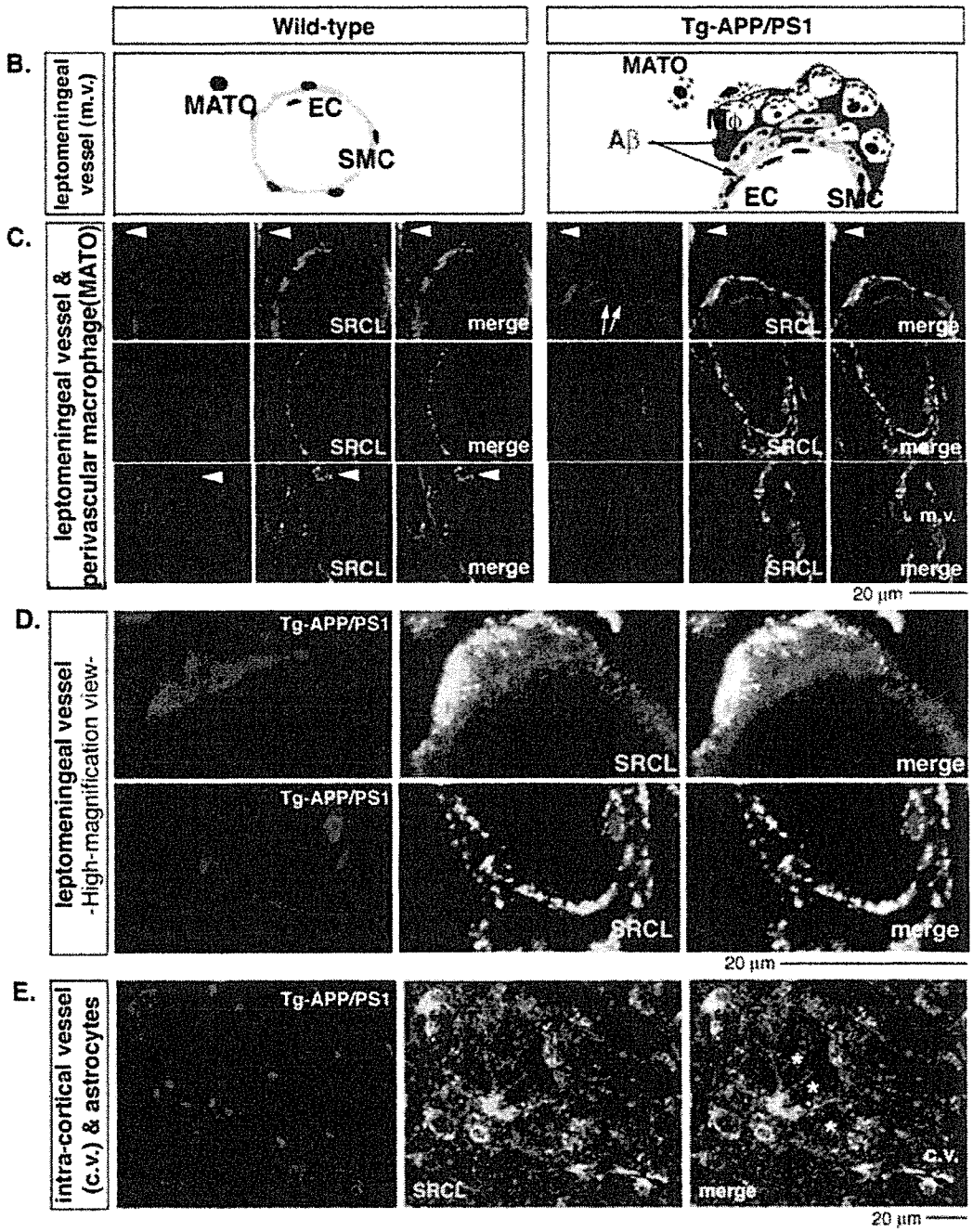

Figure 6. (Continued).

positive SMCs (red) in Tg-APP/PS1 mice (Fig. 6C, middle panel). At high-magnification (Fig. 6D, lower panel), SRCL-IR appeared as multiple particles colocalized with αSMA-IR inside cells, indicating that SMCs of Tg-APP/PS1 also internalized SRCL. We observed strong induction of SRCL-IR (green) within both GFAP-positive astrocytic cell bodies (red) and their end feet (red) surrounding a cortical vessel (c.v.) associated with cerebral amyloid angiopathy (CAA) in Tg-APP/PS1 (Fig. 6E). The astrocytes associated with Aβ-plaques (asterisks) expressed SRCL-IR predominantly intracellularly, suggesting the internalization, of Aβ by SRCL in

astrocytes. Interestingly, we could occasionally observe astrocytes that extended their feet toward both an amyloid plaque (asterisk) and cortical micro-vessels (c.v.). This finding may suggest a possible role of astrocytic SRCL for Aβ clearance by transfer from amyloid plaque to the systemic circulation via c.v.

In brief summary, immunostaining results showed that, in wild-type littermates, SRCL-IR was present in MATO cells and to a lesser extent in SMCs, whereas SRCL-IR was markedly induced and colocalized with $fA\beta_{1-40/1-42}$-IR as particles inside the vascular wall. Within the vascular/perivascular cells, SRCL was induced in infiltrating macrophages, MATO cells, SMCs, ECs and astrocytes in Tg-APP/PS1, thus raising the possibility that upregulated SRCL in subpopulations of vascular/perivascular cells may play an important role in the binding, and presumably the clearance, of Aβ in the Tg-APP/PS1 brain.

Real-Time RT-PCR Shows the Expression of SRCL in the Brain of Patients With AD

To assess the expression and localization of SRCL in the brains of AD patients, we examined *SRCL* mRNA expression in autopsy samples from patients with AD and control subjects listed in Figure 7A. Although the number of autopsy samples was limited and thus insufficient for statistical analysis, quantitative real-time RT-PCR showed a tendency for an increase in the level of the *SRCL* mRNA in the cortical tissues of AD patients compared to the level in the control subjects (Fig. 7B), suggesting a role for SRCL in AD brain.

Expression of hSRCL in Brains of Patients With AD

We investigated the immunolocalization of SRCL in the temporal cortex of patients with AD. A large number of SRCL-IR cells were present in AD brain tissues, whereas SRCL-IR cells were rare in control samples (Fig. 8A). Using SRCL/GFAP-double immunostaining, we observed that strong SRCL-IR (pink) was colocalized with GFAP-IR (brown) in plaque (black asterisks)-surrounding reactive astrocytes and in perivascular astrocytic end-feet (brown) associated with CAA (green asterisks) in the temporal cortex of AD-affected brains (Fig. 8B). At high magnification, SRCL-IR appeared as particles within the cells (Fig. 8B, right panel). Furthermore, when we stained for SRCL and Iba-1 (for microglia/macrophages including MATO cells), SRCL-IR (pink) was found in some Iba1-positive activated microglia (arrows) or vascular macrophages and MATO cells (arrowhead) in the AD-affected brains (Fig. 8C). In addition, double immunostaining for SRCL (pink) and $A\beta_{1-40/1-42}$ (brown) showed that SRCL-IR was colocalized with Aβ as multiple particles in intracellular compartments of vascular cells, such as infiltrating macrophages, SMCs, and some ECs in the AD samples (Fig. 8D,E, in green arrowheads) consistent with the findings in Tg-APP/PS1 (Fig. 6A,D). The specificity of

A

Disorder	Age	Sex	Cause of death
Control	79	F	drug overdose
Control	71	F	multiple medical disorder
Control	20	M	multiple injuries
AD	81	M	complication of AD
AD	87	F	heart disease
AD	86	F	complication of AD
AD	83	F	complication of AD

B

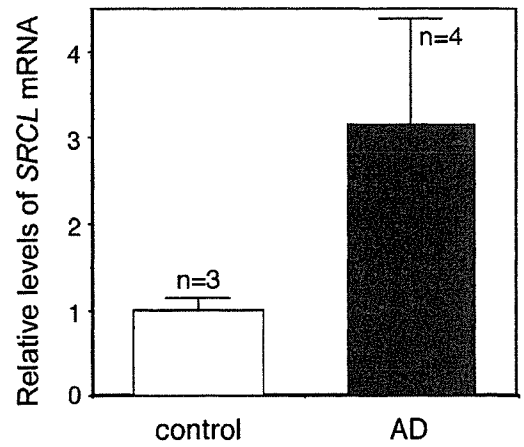

Fig. 7. Expression of *hSRCL* mRNA in brains of AD patients. **A:** Summary of autopsy samples used for analysis of *hSRCL* mRNA expression. **B:** Quantitative real-time RT-PCR of *hSRCL* mRNA from the temporal cortex of control subjects and AD patients. The *hSRCL* mRNA level was expressed as the ratio to that of *GAPDH* mRNA. Scale bar = ±SE (standard error).

SRCL-IR was confirmed by pre-absorbing the antibody with its immunogen (Fig. 8F).

In brief summary, in AD-brains, SRCL-IR appeared as numerous particles inside plaque-associated reactive astrocytes, activated microglia, and vascular/perivascular cells, such as the infiltrating macrophages within the vessel wall, SMCs and ECs that were associated with CAA and was consistent with our findings in Tg-APP/PS1 mice. Our findings thus suggest that upregulated SRCL on reactive astrocytes, activated microglia, and vascular/perivascular cells might be involved in Aβ binding and clearance in AD.

DISCUSSION

The accumulation of fibrillar Aβ (fAβ) is an important component of AD pathogenesis, a disease that

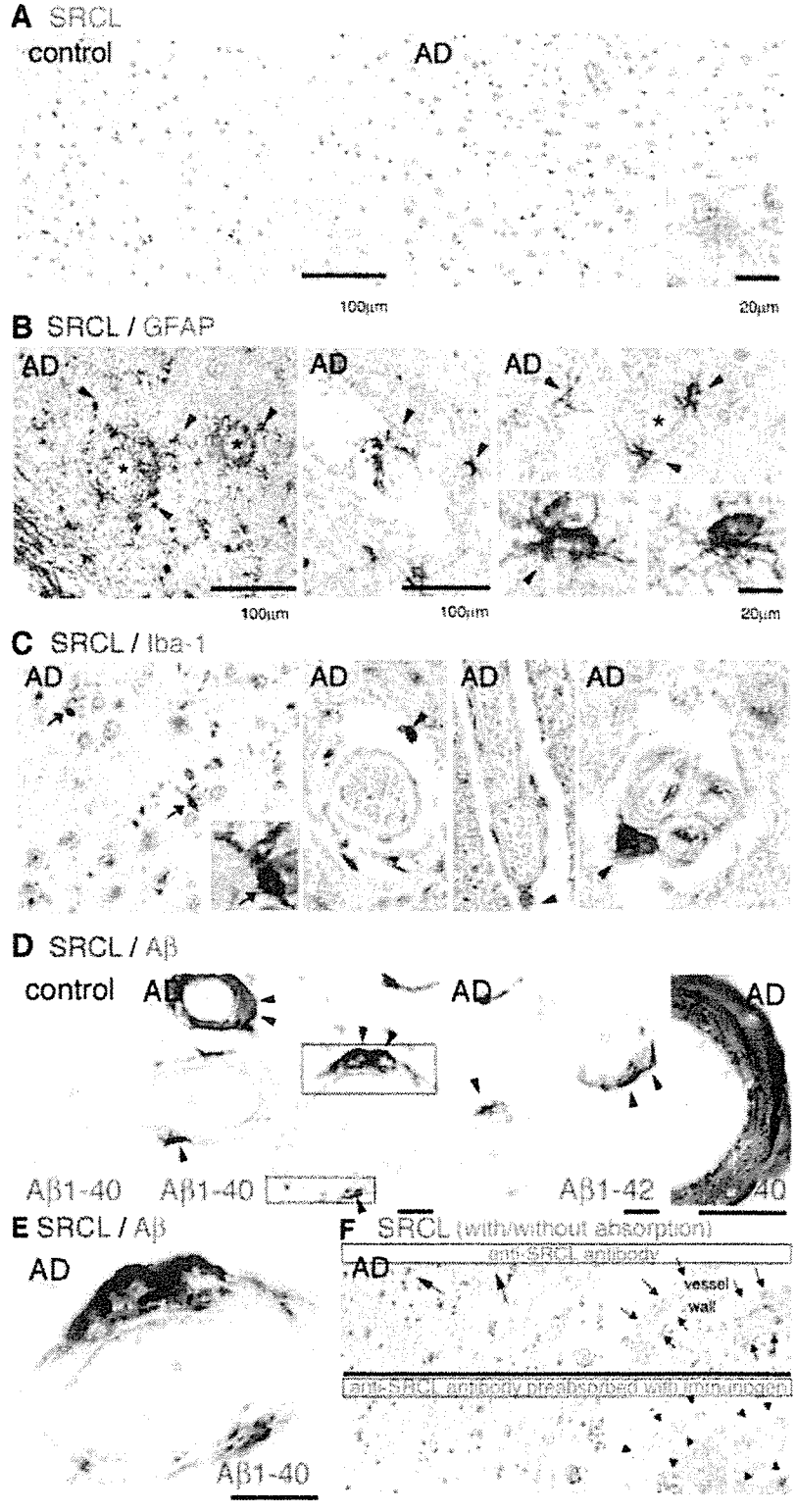

Fig. 8. Immunostaining for hSRCL in the temporal cortex of AD patients. Formalin-fixed human brain tissues from control subjects and AD patients were embedded in paraffin, deparaffinized, sectioned thinly, and used for immunostaining. **A:** Brain tissues of controls and AD patients immunostained with anti-SRCL antibody recognizing hSRCL. Immunoreactivity was visualized by using DAB (brown color). **B:** Double-immunostaining for hSRCL (pink) and GFAP (brown). Arrowheads indicate hSRCL-IR astrocytes surrounding Aβ deposits (black asterisks). Green asterisk, intra-cortical vessel. **C:** Double-immunostaining of hSRCL (pink) and Iba-1 (brown), a marker for microglia/macrophages. Arrows indicate hSRCL-IR microglial cells. Arrowheads indicate hSRCL-IR-MATO cells. **D:** Double-immunostaining of hSRCL (pink) and $A\beta_{1-42}$ (brown) in a vessel associated with CAA. Green asterisks and green arrowheads indicate vessels and hSRCL/Aβ double-positive particles, respectively. Scale bars = 20 μm. **E:** High-magnification views of rectangular areas shown in second panel of (D). Scale bar = 20 μm. Green arrowheads indicate SRCL/Aβ double positive particles; and green asterisks indicate intravascular spaces of leptomeningeal vessel. **F:** Absorption test. Immunostaining for hSRCL (brown) with or without preabsorption with immunogen. Black arrows show cells with hSRCL-IR. Black arrowheads indicate cells, the hSRCL-IR of which was eliminated by preabsorption with immunogen.

causes significant morbidity and mortality in adult populations. We wished to determine factors that may modulate accumulation of Aβ in vivo, and focused our attention on the clearance of Aβ by SRCL. Clearly, SRCL was expressed in the brains of AD patients, and SRCL could bind fAβ. RT-PCR showed that SRCL was expressed in neonatal astrocytes and microglia in tissue culture, and that *SRCL* mRNA levels increased after increased microglial activation. In addition, SRCL levels increased in neonatal astrocytes treated with fAβ in vitro. These in vitro data are consistent with immunohistochemical findings. In control mice and human subjects, SRCL-IR was below the detection limits in astrocytes, microglia and macrophages except perivascular macrophages (MATO cells). SRCL-IR intensity was elevated in most of the Aβ-positive astrocytes and in some of the Aβ-positive microglia in the brains of Tg-APP/PS1 mice and humans with AD. Interestingly, in samples obtained from the former, SRCL-IR levels were low in astrocytes that were Aβ-negative. Thus, SRCL may be important in activated glial cell function in situations of neurodegeneration such as occur in AD.

We showed that SRCL-IR was not present in endothelial cells of the healthy adult brain (mouse or human), which contrasts with findings for mouse cardiac endothelial cells (Ohtani et al., 2001). Although the reason for this difference is not clear, tissue and age differences or differences in reagents used could explain this discrepancy. In contrast to healthy brains, we observed significant SRCL-IR in endothelial cells closely associated with cerebral amyloid angiopathy (CAA) in patients with AD, suggesting a role for SRCL in Aβ-loaded (stressed) endothelial cells. In addition, we found strong SRCL-IR in smooth muscle cells and MATO cells closely associated with CAA. Our ability to observe colocalization of Aβ and SRCL in intracellular compartments of vascular cells suggests that SRCL may function in internalization/clearance of Aβ-peptide. Strong binding of $fA\beta_{1-42}$ to CHO-K1 cells that expressed SRCL further supports this hypothesis.

The mechanisms by which SRCL expression is controlled are not well understood. However, as Aβ activates a variety of transcriptional signals, such as AP-1, NF-κB and cAMP responsive element-binding protein (CREB) at Ser133, and such signals have been proposed as a mechanism for Aβ-induced changes in gene expression (McDonald et al., 1998; Yin et al., 2002; Kim et al., 2003) and because we found corresponding consensus sequences for AP-1 and NF-κB in the promoter and 5′ UTR of *SRCL*, it is possible that some of these signals in glial and vascular cells could be involved in the mechanisms regulating *SRCL* expression.

The scavenger receptors A, BI (SR-A, SR-BI), and CD36, a complex involving CD36, α(6)β(1)-integrin as well as CD47, and heparan sulfate proteoglycans on glial cells have been reported to bind Aβ. A role for these microglial scavenger receptors in the Aβ-induced activation of inflammatory responses has been proposed. However, the role of the receptors in the clearance of Aβ is not yet well understood (Verdier and Penke, 2004; Ricciarelli et al., 2004). Even in the case of suggested scavenger receptors, their contribution has been considered to be partial. For example, although microglial or astroglial binding or internalization of $fA\beta_{1-42}$ peptide mediated through other receptors has been suggested for several SR family members, including SR-AI, SR-BI, CD36, and MARCO, no single receptor has been found to be essential. Indeed, deletion of SR-A by genetic knock-out did not increase amyloid plaque formation or neurodegeneration in transgenic mice expressing human amyloid protein precursors (Huang et al., 1999), suggesting the presence of alternative receptors for glial-mediated Aβ clearance.

The vascular system also may play a role in Aβ clearance. It has been suggested that LDL receptor-related protein-1 (LRP-1), a SR that binds various ligands including apoE, α2-macroglobulin, and APP, may function in Aβ vascular transport in young mice. When $A\beta_{1-40}$ was intracerebrally administered at high concentrations, LRP-1 facilitated $A\beta_{1-40}$ transport across the blood brain barrier (BBB) into the plasma. However, when given at lower concentrations of $A\beta_{1-40}$, anti-LRP antibody did not affect the clearance of $A\beta_{1-40}$ (Shibata et al., 2000). Thus Shibata et al. suggested the presence of an alternative, highly sensitive BBB transport mechanism, in addition to LRP-1. The molecular nature of this putative second transport system is not known. Some receptors have been proposed, e.g., the receptor for advanced glycosylation end-products (RAGE) and LRP-2; but they are unlikely to be involved in the rapid clearance of Aβ from the brain, and responsible receptor has yet to be found (Shibata et al., 2000). Considering such findings, our present data suggest SRCL to be the additional receptor responsible for vascular clearance of Aβ. The fact must be considered that increased amounts of fAβ itself increases Aβ deposition in vessel walls and can importantly affect in CAA, presumably due to the Aβ-dependent regulation of the receptors responsible for Aβ clearance. As most candidate SRs, such as CD36, are indeed downregulated in the adult (aged) brain even in the healthy condition or in the AD-affected brain, they thus may not play significant roles in the late stage of AD (Husemann et al., 2002). It seems likely that upregulated SRCL in association with Aβ-plaque and CAA could play an important role in Aβ clearance in an Aβ dose-dependent manner. Other mechanisms, such as those causing decreased vessel elasticity, have been suggested to reduce the efficiency of Aβ clearance. For example, ablation of the nucleus basalis in the rabbit, the source of cholinergic innervation of blood vessels in the brain, results in CAA (Roher et al., 2000), suggesting that disturbance of blood vessel tone and pulsations could be a factor in deposition of Aβ in artery walls. Loss of elasticity in aging human cerebral arteries with progressive arteriosclerosis (Perry et al., 1998; Kalaria, 2001) or cessation of pulsations with focal thromboembolic occlusion (Weller et al., 2002) might play a role in impeding drainage of Aβ and in pathogenesis of CAA

(Weller et al., 2002). As it has been suggested that SRs are involved in attenuation of arteriosclerosis due to their capability to bind Oxy-LDL (Rigotti, 2000), and because SRCL has the ability to bind Oxy-LDL, we may postulate that upregulated SRCL on vascular cells may play a role in attenuating loss of elasticity of brain vessels in aged patients with AD, thereby indirectly improving the clearance of Aβ.

Based on all data taken together, we propose that SRCL on glial or cerebral vascular/perivascular cells functions as a physiological receptor, upregulated by Aβ and pivotally facilitating the clearance of substances such as Aβ and LDL in AD-affected brain tissues, thus attenuating disease progression. We are currently developing SRCL-null mice, and the generation and analysis of triple transgenic offspring of SRCL-null and Tg-APP/PS1 mice may clarify the contribution of SRCL and allow us to devise new approaches targeting SRCL for the clearance of Aβ in AD.

In summary, this is the first description of the upregulation and possible role of SRCL in the binding or clearance of Aβ by glial and vascular/perivascular cells associated with AD. Our findings provide a new insight into the pathophysiology of AD and suggest future SRCL-based therapeutic interventions against Aβ-mediated pathogenesis in AD.

ACKNOWLEDGMENTS

We are grateful to Dr. Checler for kindly providing anti-Aβ antibodies (rabbit anti-Aβ40 (FCA3340) and anti-Aβ42 (FCA3542) antibodies). We are also grateful to Dr. Kadoyama for the help with astrocyte cultures and Dr. Kanzaki for the generation of CHO-K1 cells stably expressing mSRCL-Flag. This work was supported in part by research grants from COE to T.N., and by grants from the Ministry of Education, Science, Technology, Sports and Culture of Japan and Ministry of Health and Welfare of Japan to T.N. and H.F.

REFERENCES

Alarcon R, Fuenzalida C, Santibanez M, von Bernhardi R. 2005. Expression of scavenger receptors in glial cells. Comparing the adhesion of astrocytes and microglia from neonatal rats to surface-bound beta-amyloid. J Biol Chem 280:30406–30415.

Bard F, Cannon C, Barbour R, Burke RL, Games D, Grajeda H, Guido T, Hu K, Huang J, Johnson-Wood K, Khan K, Kholodenko D, Lee M, Lieberburg I, Motter R, Nguyen M, Soriano F, Vasquez N, Weiss K, Welch B, Seubert P, Schenk D, Yednock T. 2000. Peripherally administered antibodies against amyloid beta-peptide enter the central nervous system and reduce pathology in a mouse model of Alzheimer disease. Nat Med 6:916–919.

DeMattos RB, Bales KR, Cummins DJ, Paul SM, Holtzman DM. 2002. Brain to plasma amyloid-beta efflux: a measure of brain amyloid burden in a mouse model of Alzheimer's disease. Science 295:2264–2267.

El Khoury JB, Moore KJ, Means TK, Leung J, Terada K, Toft M, Freeman MW, Luster AD. 2003. CD36 mediates the innate host response to beta-amyloid. J Exp Med 197:1657–1666.

Funakoshi H, Okuno S, Fujisawa H. 1991. Different effects on activity caused by phosphorylation of tyrosine hydroxylase at serine 40 by three multifunctional protein kinases. J Biol Chem 266:15614–15620.

Funakoshi H, Yonemasu T, Nakano T, Matumoto K, Nakamura T. 2002. Identification of Gas6, a putative ligand for Sky and Axl receptor tyrosine kinases, as a novel neurotrophic factor for hippocampal neurons. J Neurosci Res 68:150–160.

Guenette SY. 2003a. Astrocytes: a cellular player in Abeta clearance and degradation. Trends Mol Med 9:279–280.

Guenette SY. 2003b. Mechanisms of Abeta clearance and catabolism. Neuromolecular Med 4:147–160.

Hsiao K, Chapman P, Nilsen S, Eckman C, Harigaya Y, Younkin S, Yang F, Cole G. 1996. Correlative memory deficits, Abeta elevation, and amyloid plaques in transgenic mice. Science 274:99–102.

Huang F, Buttini M, Wyss-Coray T, McConlogue L, Kodama T, Pitas RE, Mucke L. 1999. Elimination of the class A scavenger receptor does not affect amyloid plaque formation or neurodegeneration in transgenic mice expressing human amyloid protein precursors. Am J Pathol 155: 1741–1747.

Husemann J, Loike JD, Anankov R, Febbraio M, Silverstein SC. 2002. Scavenger receptors in neurobiology and microglia and other cells of the nervous system. Glia 40:195–205.

Kakimura J, Kitamura Y, Takata K, Umeki M, Suzuki S, Shibagaki K, Taniguchi T, Nomura Y, Gebicke-Haerter PJ, Smith MA, Perry G, Shimohama S. 2002. Microglial activation and amyloid-beta clearance induced by exogenous heat-shock proteins. FASEB J 16:601–603.

Kalaria RN. 2001. Advances in molecular genetics and pathology of cerebrovascular disorders. Trends Neurosci 24:392–400.

Kim JY, Kim H, Lee SG, Choi BH, Kim YH, Huh PW, Lee KH, Han H, Rha HK. 2003. Amyloid beta peptide (Abeta42) activates PLC-delta1 promoter through the NF-kappaB binding site. Biochem Biophys Res Commun 310:904–909.

Kodama T, Freeman M, Rohrer L, Zabrecky J, Matsudaira P, Krieger M. 1990. Type I macrophage scavenger receptor contains alpha-helical and collagen-like coiled coils. Nature 343:531–535.

Koistinaho M, Lin S, Wu X, Esterman M, Koger D, Hanson J, Higgs R, Liu F, Malkani S, Bales KR, Paul SM. 2004. Apolipoprotein E promotes astrocyte colocalization and degradation of deposited amyloid-beta peptides. Nat Med 10:719–726.

Matsuoka Y, Saito M, LaFrancois J, Gaynor K, Olm V, Wang L, Casey E, Lu Y, Shiratori C, Lemere C, Duff K. 2003. Novel therapeutic approach for the treatment of Alzheimer's disease by peripheral administration of agents with an affinity to beta-amyloid. J Neurosci 23:29–33.

McDonald DR, Bamberger ME, Combs CK, Landreth GE. 1998. beta-Amyloid fibrils activate parallel mitogen-activated protein kinase pathways in microglia and THP1 monocytes. J Neurosci 18:4451–4460.

Murphy JE, Tedbury PR, Homer-Vanniasinkam S, Walker JH, Ponnambalam S. 2005. Biochemistry and cell biology of mammalian scavenger receptors. Atherosclerosis 182:1–15.

Nakamura K, Funakoshi H, Miyamoto K, Tokunaga F, Nakamura T. 2001a. Molecular cloning and functional characterization of a human scavenger receptor with C-type lectin (SRCL), a novel member of a scavenger receptor family. Biochem Biophys Res Commun 280:1028–1035.

Nakamura K, Funakoshi H, Tokunaga F, Nakamura T. 2001b. Molecular cloning of a mouse scavenger receptor with C-type lectin (SRCL)(1), a novel member of the scavenger receptor family. Biochim Biophys Acta 1522:53–58.

Nakano Y, Kondoh G, Kudo T, Imaizumi K, Kato M, Miyazaki JI, Tohyama M, Takeda J, Takeda M. 1999. Accumulation of murine amyloidbeta42 in a gene-dosage-dependent manner in PS1 'knock-in' mice. Eur J Neurosci 11:2577–2581.

Naveilhan P, Neveu I, Baudet C, Funakoshi H, Wion D, Brachet P, Metsis M. 1996. 1, 25-Dihydroxyvitamin D3 regulates the expression of the low-affinity neurotrophin receptor. Brain Res Mol Brain Res 41:259–268.